CO_2 Capture by Absorption with Potassium Carbonate
Second Quarterly Report 2006

Quarterly Progress Report
Reporting Period Start Date: April 1, 2006
Reporting Period End Date: June 30, 2006
Authors: Gary T. Rochelle, Eric Chen, Babatunde Oyenekan,
Andrew Sexton, Jason Davis, Marcus Hilliard, Amornvadee Veawab

July 28, 2006
DOE Award #: DE-FC26-02NT41440
Department of Chemical Engineering
The University of Texas at Austin

Disclaimer

This report was prepared as an account of work sponsored by an agency of the United States Government. Neither the United States Government nor any agency thereof, nor any of their employees, makes any warranty, express or implied, or assumes any legal liability or responsibility for the accuracy, completeness, or usefulness of any information, apparatus, product, or process disclosed, or represents that its use would not infringe privately owned rights. Reference herein to any specific commercial product, process, or service by trade name, trademark, manufacturer, or otherwise does not necessarily constitute or imply its endorsement, recommendation, or favoring by the United States Government or any agency thereof. The views and opinions of authors expressed herein do not necessarily state or reflect those of the United States Government or any agency thereof.

Abstract

The objective of this work is to improve the process for CO_2 capture by alkanolamine absorption/stripping by developing an alternative solvent, aqueous K_2CO_3 promoted by piperazine. The pilot plant data have been reconciled using 17% inlet CO_2. A rate-based model demonstrates that the stripper is primarily controlled by liquid film mast transfer resistance, with kinetics at vacuum and diffusion of reactants and products at normal pressure. An additional major unknown ion, probably glyoxylate, has been observed in MEA degradation. Precipitation of gypsum may be a feasible approach to removing sulphate from amine solutions and providing for simultaneous removal of CO_2 and SO_2. Corrosion of carbon steel in uninhibited MEA solution is increased by increased amine concentration, by addition of piperazine, and by greater CO_2 loading.

Contents

List of Figures

List of Tables

Introduction

The objective of this work is to improve the process for CO_2 capture by alkanolamine absorption/stripping by developing an alternative solvent, aqueous K_2CO_3 promoted by piperazine. This work expands on parallel bench-scale work with system modeling and pilot plant measurements to demonstrate and quantify the solvent process concepts.

Gary Rochelle is supervising the bench-scale and modeling work; Frank Seibert is supervising the pilot plant. Three graduate students (Babatunde Oyenekan, Ross Dugas, Jason Davis) have received support during this quarter for direct effort on the scope of this contract. Three students supported by other funding have made contributions this quarter to the scope of this project (Eric Chen – EPA Star Fellowship; Marcus Hilliard, Andrew Sexton – Industrial Associates). Subcontract work was performed at the University of Regina under the supervision of Amy Veawab.

Experimental

Subtask 1.2 describes the operating procedure for the wetted wall column.

Subtask 1.8 describes a rate-based model to predict stripper performance.

Subtask 3.1 presents methods for analyzing amine degradation products by anion and cation chromatography.

Subtask 3.3 describes planned procedures for measuring thermal degradation of amines.

Subtask 3.4 describes methods to reconcile measured temperature and water vapor pressure in the apparatus for measuring amine volatility.

Subtask 4.1 describes a method for measuring the rate of calcium hydroxide dissolution in buffered amine solution.

Task 5 describes electrochemical methods for measuring corrosion.

Results and Discussion

Progress has been made on five subtasks in this quarter:

Subtask 1.8 – Predict Flowsheet Options

The rate-based model has been used to compare stripper performance and normal pressure and vacuum and to study the influence of stripper diameter on energy cost.

Subtask 2.6 – Campaign 4

The results of campaign 4 have been reconciled with an inlet CO_2 of 17% rather than 12% to compensate for an error in interpreting the CO_2 concentration units of calibration cylinders. With this interpretation the material balances are in better agreement. The approximate values of the mass transfer coefficient are about half of those expected from bench-scale measurements.

Subtask 3.1 – Analysis of Degradation Products

Previous samples of degraded solutions have been reanalyzed with refined quantitative methods of ion chromatography.

Subtask 3.4 – Amine Volatility

A correlation has been developed to correct the measured temperature to match the measured vapor pressure of pure water.

Subtask 4.1 – Sulfate Precipitation

The rate of dissolution of calcium hydroxide was measured in MEA solutions at pH 10 and pH 11.

Subtask 5.1 – Corrosion in base solution compared to MEA

Corrosion measurements have been performed with 5 to 8.7 M amine with 0 to 0.25 moles PZ/mole amine with lean and rich CO_2 loading at 80^{o}C.

Conclusions

1. A "short and fat" stripper will require less energy that a "tall and skinny" stripper without much more packing volume.

2. The stripper is controlled by liquid film resistance. A vacuum stripper is controlled by mass transfer with fast reaction. A stripper at normal pressure is controlled by diffusion of reactants and products.

5. Acetate, glycolate, formate, oxalate, nitrite, nitrate have been quantified in both MEA and PZ degradation. An additional unknown, probably glyoxylic acid is present at significant quantities in degraded solutions of MEA.

6. Ethylenediamine has been quantified in PZ degradation.

6. The proprietary inhibitor A significantly reduces degradation products from MEA.

7. MEA degradation in the presence of iron alone produces more nitrate and nitrite. With copper present, there is more formate and less glycolate.

8. The rate of piperazine oxidative degradation is slower than the rate of MEA oxidative degradation.

9. Calcium hydroxide solids will dissolve almost completely in less than 2 hours in MEA buffered at pH 10 or 11 with HCl or H_2SO_4.

10. Corrosion of carbon steel without inhibitors increases from 16 to 26 mpy as MEA increases from 5 to 8.7 M with 0.2 moles CO2/mole amine. In 7 M MEA/1.7 M PZ the corrosion rate increase further to 35 mpy. This solution saturated to CO_2 corrodes even faster at 136 mpy.

Future Work

We expect the following accomplishments in the next quarter:

Subtask 1.1 – Modify Vapor-Liquid Equilibrium (VLE) Model

VLE data will be obtained for MEA and MEA/PZ with the hot gas FTIR.

Subtask 1.7 – Simulate and Optimize Packing Effects

The absorber data from campaigns 1, 2, and 4 will be simulated with a Ratesep model.

Subtask 1.8 – Predict Flowsheet Options

The rate-based model will be used with other stripper configurations.

Subtask 3.1 – Analysis of Degradation Products

Three additional unknown peaks from ion chromatography will be identified.

Work will start on the development of a HPLC method for thermal degradation products of MEA and PZ.

Subtask 3.3 – Thermal Degradation

Samples of loaded MEA and potassium carbonate/PZ will be degraded at 150-180 ºC.

Subtask 4.1 – Sulfate Precipitation

The solubility of potassium sulfate solids will be measured in MEA solutions.

Task 1 – Modeling Performance of Absorption/Stripping of CO2 with Aqueous K2CO3 Promoted by Piperazine

Subtask 1.2 – Modify Point Rate Model

by Ross Dugas

(Supported by this contract)

Summary

The wetted wall column has been prepared for rate measurements using amine blends of monoethanolamine and piperazine. Most of the background calibrations on the supporting equipment (mass flow controllers, Horiba CO_2 analyzers) have been completed. Since no standard operating procedure for the wetted wall column was available, one has been prepared. This standard operating procedure is still tentative since no rate measurements have yet been made. This operating procedure will be adjusted as needed.

Tentative Standard Operating Procedure for the Wetted Wall Column

Total Organic Carbon (TOC) and Horiba Gas Analyzers Preparation

1. Make sure the TOC is connected to the low range Horiba CO_2 analyzer.
2. Follow the previously developed standard operating procedure for the preparation and calibration of the TOC and low range Horiba CO_2 analyzer.
3. Using the developed mass flow controller calibrations, calibrate the high range Horiba with CO_2 and nitrogen.

Wetted Wall Column Preparation

1. Prepare the amine solution with the desired CO_2 loading.
2. Make sure the gas saturation cell is filled with water.
3. Turn on all the temperature baths to the desired temperature.
4. Verify that all the old solution has been emptied from the wetted wall apparatus. New solution may be needed to flush the tubing.
5. Load the new solution into the apparatus.
6. Allow a gas and the amine solution to flow through the column.
7. Inject solution as necessary to remove all the air space from the liquid tubing.
8. Shut off the gas and the solution pump.

Wetted Wall Column Data Collection

1. Check the solution loading three times using the TOC sample preparation standard operating procedure.
2. Choose a CO_2 concentration which is about twice the partial pressure of the solution at the desired wetted wall column pressure.
3. Let the solution flow through the wetted wall apparatus.
4. Make sure the gas outlet is connected to the appropriate Horiba CO_2 analyzer.
5. Using the mass flow controller calibrations set the gas flow to this absorption condition. Record this inlet CO_2 concentration.

6. Record the outlet CO_2 concentration from the Horiba.
7. Stop the gas and liquid flow.
8. Check the solution loading three times using the TOC sample preparation standard operating procedure. Adjust the solution loading if it has significantly deviated from the original loading.
9. Run this wetted wall column data collection procedure again alternating between absorption and desorption runs. One set of absorption/desorption runs should have CO_2 partial pressures that are a factor of 2 from equilibrium. The other set of absorption/desorption runs should have CO_2 concentrations a factor of 5 from equilibrium.

Subtask 1.8 – Rate-based Modeling – Aspen Custom Modeler for Stripper

by Babatunde Oyenekan

(Supported by this contract)

Introduction

We have continued to develop the stripper submodel in Aspen Custom Modeler for the overall model of CO_2 absorption/stripping for 7m monoethanolamine (MEA), 5m K^+ / 2.5m PZ and some generic solvents. In this work, we present rate model results for the stripping of CO_2 from a 5m K^+/2.5m PZ solvent using IMTP #40 packing at 30 kPa and 160 kPa reboiler pressures. We have used the model to determine mass transfer mechanisms in the stripper and initiated optimization of the packing volume. A 'short and fat' stripper was found to be preferable to a 'tall and skinny' one. The vacuum stripper requires less equivalent work than the simple stripper when run at the same percent flood. The results show that the stripper is liquid film controlled. The stripper operation is kinetics controlled at 30 kPa and diffusion controlled at 160 kPa.

Experimental (Model Formulation)

Stripping can occur by three mechanisms in the stripper. These are flashing, which occurs at the stripper inlet and at the top section of the stripper leading to the generation of a lot of bubbles and mass transfer area, normal mass transfer on the surface of packings or on trays and under boiling conditions in the reboiler. Modeling of stripping columns are essential so that the operation of the column could be understood, the energy requirement for stripping (which has been estimated to be ~ 80% of the operating cost of the absorption/stripping system) can be reduced and so as to provide some understanding into the phenomenon of mass transfer with chemical reaction at stripper conditions. Three main approaches are used in stripper modeling – equilibrium-stage modeling, mass transfer with equilibrium reactions and mass transfer with reaction in the boundary layer and liquid diffusion.

Equilibrium Modeling

In this approach, infinite mass transfer is assumed. The stripping column is divided into a user-defined number of sections assumed to be well mixed in the liquid and vapor phases. The reboiler is assumed to be an equilibrium stage. Murphree efficiencies are assigned to components and temperature to account for the departure from equilibrium. This approach is useful in carrying out quick evaluations of process concepts but does not describe a real process. Only the

conventional MESH (material, equilibrium, summation and enthalpy) equations are solved using this approach. This approach has been used in our previous work[1, 2].

Rate (non-equilibrium) Modeling

This approach takes into account that the rate of desorption is finite and that the transfer of CO_2 is governed by mass transfer rate and not equilibrium considerations. In addition to the conventional MESH equations, the mass and heat transfer rate equations are solved. Since these equations require physical properties, reaction rate parameters and contactor specific information. Rate-based modeling allows for insight into the fundamental mechanisms of mass transfer and could help predict the operation of a constant diameter column as well as aid in the design of columns with variable diameter at constant percent flood.

Mass Transfer with reaction in the boundary layer and liquid diffusion.

This mechanism shown in Figure 1, assumes that the CO_2 diffuses from the bulk liquid through the liquid film to the reaction film, where it reacts with the amine, and subsequently diffuses through the gas film into the bulk gas. The reaction film is close to the gas-liquid interface. It is postulated that CO_2 absorption/desorption in amines, potassium carbonate and mixtures of PZ/K_2CO_3 follow this mechanism. This approach is used in this work.

Mass Transfer with equilibrium reaction.

This mechanism shown in Figure 2 assumes that the reaction film in Figure 1 is very close to the gas liquid interface that the reaction can be assumed to occur at the gas-liquid interface. Using this mechanism, the mass transfer process can be described in terms of diffusion alone with no consideration of the kinetics of the reactions. This approach has been used by previous authors [3-5].

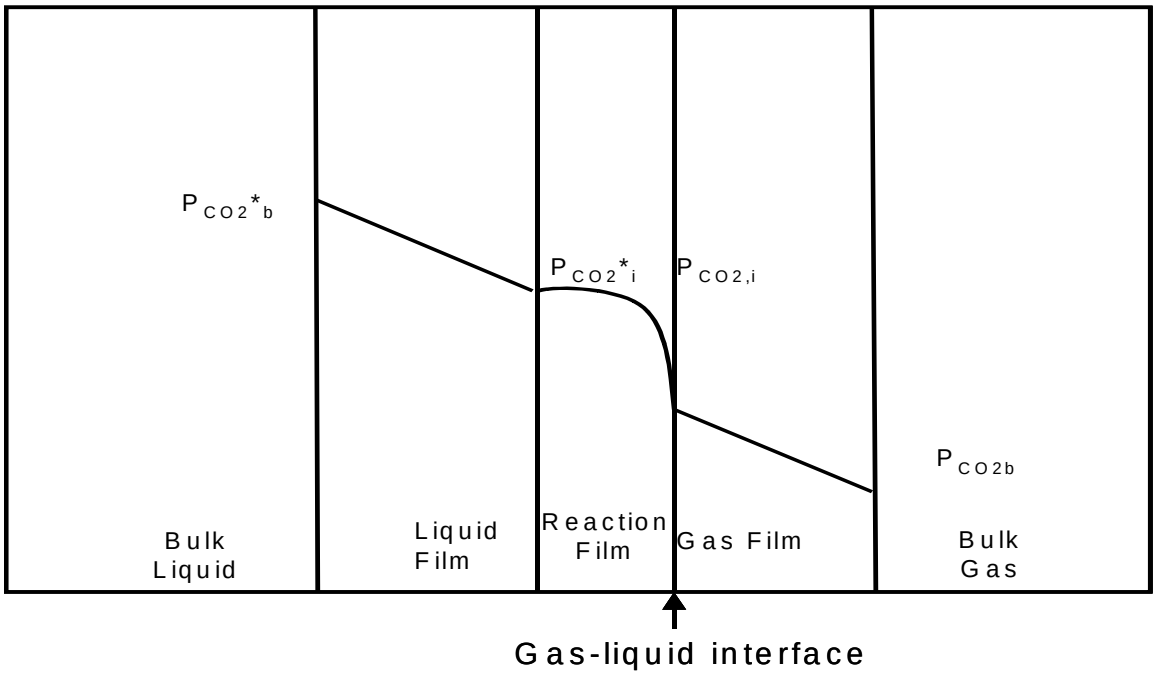

Figure 1: Mass transfer with reaction in the boundary layer and liquid diffusion

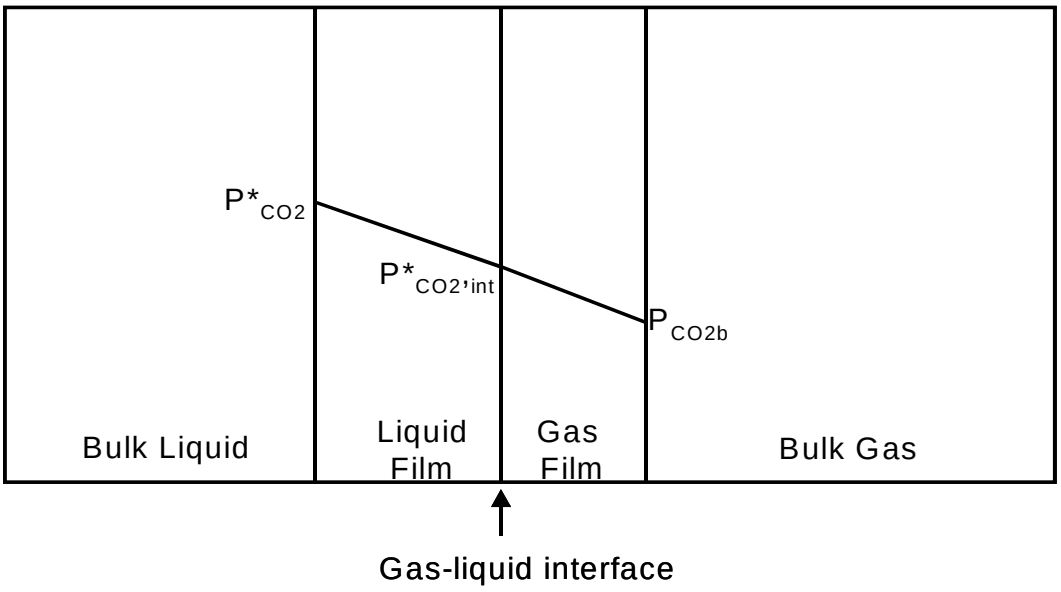

Figure 2: Mass transfer with equilibrium reaction

Aspen Custom Modeler (ACM) Model

A rate-based model has been developed in Aspen Custom Modeler to simulate the stripper operation equipped with random packing. This model has the following features:

(a) rigorous thermodynamics is accounted for by an equation regressed from results from the E-NRTL model of Chen et al.[6, 7].

(b) approximate representations of mass transfer with combined reaction.

(c) gas and liquid film mass transfer resistances are taken into account.

(d) Unequal flux of CO_2 and H_2O is accounted for in both phases.

(e) The final pressure of the CO_2 is 1000 kPa. This compression is carried out in five stages with intercooling to 313K.

Modeling Assumptions

(a) The ten sections in to which the packed section is divided are well mixed in the liquid and vapor phases.

(b) The reboiler is assumed to be an equilibrium stage.

(c) There is negligible vaporization of the solvent.

(d) The reaction takes place in the liquid phase.

The CO_2 vapor pressure (kPa) under stripper conditions for the 5m K^+/2.5m PZ solvents is given by Table 1:

Table 1: Adjustable constants in VLE expression.

$$\ln P_{CO2}^{*} = a + b^{*}ldg + \frac{c}{T} + d\frac{ldg^2}{T^2} + e\frac{ldg}{T^2} + f\frac{ldg}{T}$$

a	-4.5924	d	-1747284
b	34.2151	e	-1712091
c	-3834.67	f	8186.474

The loadings in terms of total alkalinity at different equilibrium partial pressures of CO_2 at 40^oC for 5m K^+/2.5m PZ are given in Table 2.

Table 2: Loadings at different equilibrium partial pressures of CO_2 at 40^oC.

P_{CO2}* (kPa)	**CO_2 loading** $\left[\frac{\text{mol } CO_2}{\text{mol } K^+ + \text{mol } 2^*PZ}\right]$
0.125	0.416
0.250	0.441
0.500	0.467
1.000	0.494
1.250	0.503
2.500	0.531
5.000	0.560
10.000	0.592

The performance of the strippers is expressed in terms of equivalent work. This is done to compare the different configurations on the same bases as well as to be able to quantify contributions from two forms of energy, heat and work. The equivalent work for stripping is given by the expression:

$$W \text{ (kJ/gmol } CO_2) = 0.75\ Q\left[\frac{T_{cond} - 313}{T_{cond}}\right] + W_{comp} + W_{pump} \quad (1)$$

T_{cond} is the temperature of condensing steam, set at 10K greater than the reboiler temperature, W_{comp} is the work of compression with a 75% efficiency and W_{pump} is the work required by the pumps with a 65% efficiency.

The flux of CO_2 is given by the expression

$$N_{CO2} = K_G (P_{CO2}^* - P_{CO2}) \quad (2)$$

The overall mass transfer coefficient (K_G) is the sum of the gas phase (k_g) and liquid phase (k_g') components.

$$\frac{1}{K_G} = \frac{1}{k_g} + \frac{1}{k_g'} \quad (3)$$

The hydraulic parameters k_ga, kla are obtained form Onda[8] while a was obtained from tests at the University of Texas Separations Research Program. The liquid phase mass transfer coefficient defined in terms of partial pressure driving forces, k_g', is calculated by an equation regressed from Cullinane [9] and is a function of the loading, temperature and partial pressure of CO_2 at the interface.The CO_2 desorption rate is:

$$\text{Rate} = K_G A (P_{CO2}^* - P_{CO2}) \quad (4)$$

The wetted area of contact, A, depends on the equipment and hydraulics in the column.

The overall mass transfer coefficient, K_G, for mass transfer with reaction in the boundary layer and liquid diffusion is given by:

$$\frac{1}{K_G} = \frac{1}{k_g} + \frac{H_{CO2}}{\sqrt{k_2 [Am]_i D_{CO2}}} + \frac{1}{k_{l,prod}} \left(\frac{\Delta P_{CO2}}{\Delta [CO_2]_T} \right)^* \quad (5)$$

with H_{CO2} being the Henry's law constant for CO_2,k_2, the reaction rate constant, [Am]I, the concentration of amine at the interface, D_{CO2}, the diffusivity of CO_2, $k_{l,\ prod}$, the liquid mass transfer coefficient of the products which is assumed to be equal for all products, $[CO_2]_T$, the total concentration of CO_2 in all forms. The term in the bracket in the third term on the right hand side of equation 5 is the secant of the equilibrium curve. If the reaction occurs very fast so that the rate constant, k_2, is very large, then the second term on the right hand side of equation (4) drops out and we have the expression for K_G for mass transfer with equilibrium reaction given by:

$$\frac{1}{K_G} = \frac{1}{k_g} + \frac{1}{k_{l,prod}} \left(\frac{\Delta P_{CO2}}{\Delta [CO_2]_T} \right)^* \quad (6)$$

The model inputs were the rich and lean loadings, the liquid rate, the temperature approach in the cross exchanger (difference between the temperature of the rich stripper feed and the lean

solution leaving the bottom of the stripper), and column pressure. Initial guesses of the segment temperatures, partial pressures, and loadings were provided. The model solves the MESH equations, the mass and energy transfer rate equations and calculates temperature and composition profiles, reboiler duty, and equivalent work.

Results and Discussion

Predicted Stripper Performance from Rate-Based Model

For a rate-based (non-equilibrium) model, the percent flood was specified. For a specified rich and lean loading, 0.560 (rich) and 0.467 (lean) mol CO_2/mol Total Alkalinity, the diameter and height of the column required to achieve the separation with a fixed volume of packing was calculated. The results are shown in Table 3. At a fixed percent flood, a 'short and fat' column is required to perform the separation in the vacuum stripper relative to the simple stripper. The reboiler duty is higher with the vacuum stripper but since the steam required to drive the reboiler has a less work value under vacuum conditions (30 kPa) than at 160 kPa, the total equivalent work is less with the vacuum stripper even though the work of compression is more. At a fixed percent flood, the vacuum stripper operation requires ~ 7% less equivalent work than the simple one.

Table 3: "Short and Fat" vs. "Tall and Skinny" Column

(5m K^+/2.5m PZ, L=30 gpm, Rich ldg = 0.560, Lean ldg = 0.467 mol CO_2/mol Total Alk, Tapp = 5^{o}C, Fixed Volume of Packing = 0.858 m^3)

Reboiler P	% flood	D	H	Q_{reb}	W_{comp}	Total W_{eq}
kPa		m		kJ/mol		
30	80	0.33	9.8	190	18	33.7
	30	0.51	4.2	155	15	30.9
160	80	0.20	26.8	138	7.6	35.3
	30	0.33	10.2	128	7	33.3

McCabe-Thiele plots give an indication of the internal operation of the column and could help understand column behavior. The McCabe-Thiele plot for the vacuum stripper is shown in Figure 3. The rich solution flashes at the top of the stripper and the temperature drops at the rich end. The top half of the column is pinched. The bottom half exhibits a well defined driving force. The bulk of the stripping operation takes place in the reboiler. This could be a consequence of the reboiler being treated as an equilibrium stage in the model. The McCabe-Thiele plot for the simple stripper is shown in Figure 4. The rich solution flashes to a much greater degree than in the vacuum case. This is because the pressure and temperature are higher and as such the partial pressure of the rich solution is significantly higher in the simple stripper than in the vacuum case. The stripping operation occurs mainly as a result of flashing and in the reboiler. This may constitute a sub-optimal case as this implies that the amount of packing used in this stripper is a lot more than required and as such there are sections of packing in which little or no stripping occurs.

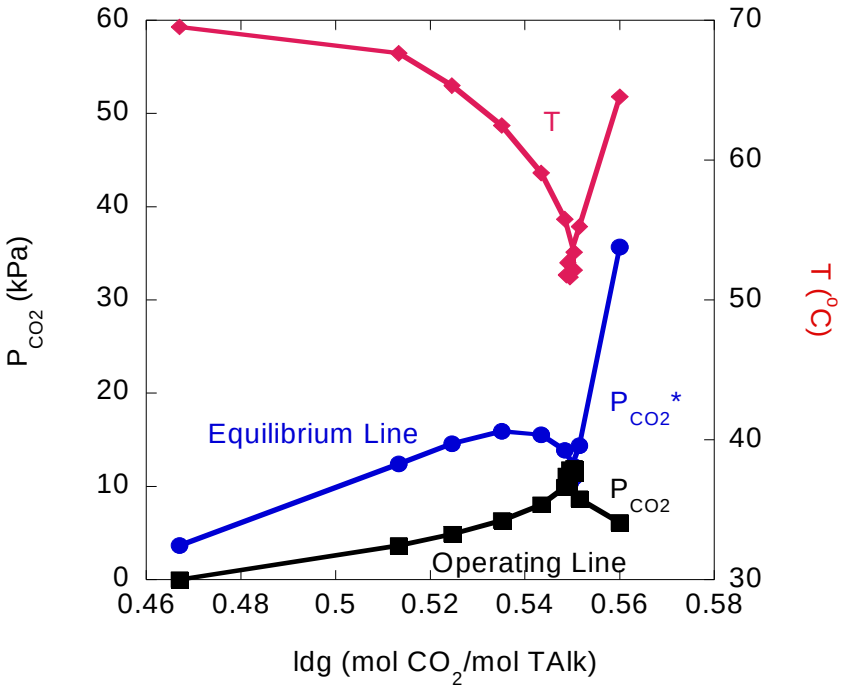

Figure 3: McCabe-Thiele plot for vacuum stripper (Rich ldg= 0.560, lean ldg= 0.467, T_{app}= 5°C)

The mass transfer mechanisms in the stripper were also investigated. The liquid phase mass transfer coefficient, k_y', and the overall mass transfer coefficient, K_y', based on mole fraction units for the vacuum and simple strippers are shown in Table 4. The results show that the rates increase from the rich to the lean end by over a factor of 2 for the vacuum case and about 1.5 for the simple case. The rate increases because as we go done the column from the rich end to the lean end, there is more free amine available for reaction. The rates in the simple stripper are also an order of magnitude greater than the vacuum case. This is as a result of the high temperatures than increase the reaction rate constant at high pressures. The table also shows that kinetic resistance has the largest contribution (89% at the rich end and 60% at the lean end) to the overall mass transfer rate under vacuum conditions while the diffusion of products is more important in the simple stripper accounting for 69% at the rich end and 50% at the lean end.

Conclusions and Future Work

In this quarter, a rate model was developed in Aspen Custom Modeler (ACM). This model was used to determine favorable design orientations for the stripper and understand mass transfer mechanisms for stripping operations using 5m K^+/2.5m PZ as the solvent. The results show that a 'short and fat' stripper is more attractive than a 'tall and skinny one'. The pressure drop is also less with a 'short and fat' stripper. At a fixed percent flood, the vacuum stripper requires ~ 7% less equivalent work than the simple one. The stripper operation was found to be liquid film controlled. The vacuum stripper was kinetic controlled while the simple stripper was diffusion controlled.

In the next quarter, the packing volume will be optimized and the pilot plant campaign results will be revisited in order to interpret the results, which will help in the fine-tuning of the model.

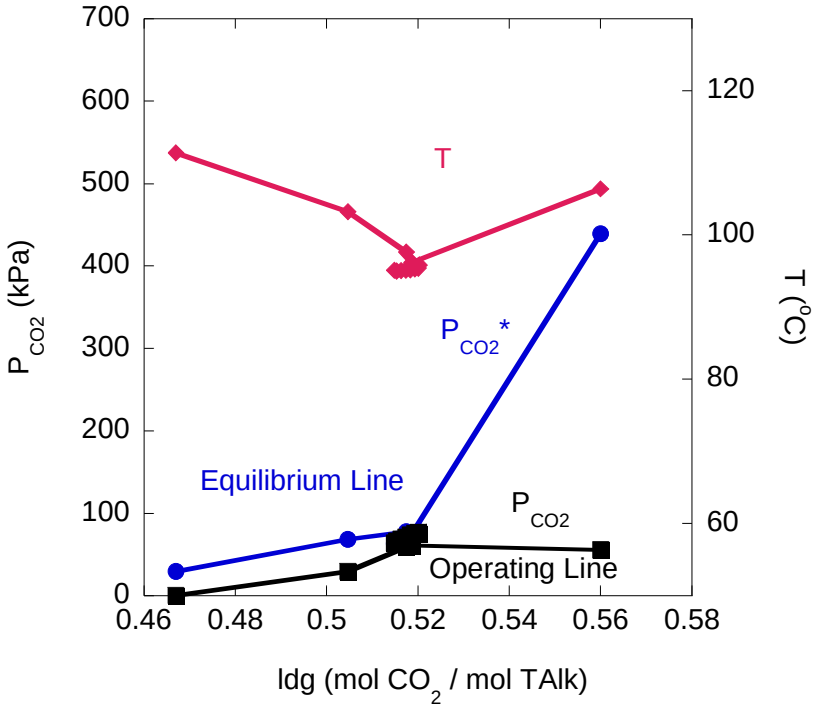

Figure 4: McCabe-Thiele plot for simple stripper (Rich ldg = 0.560, lean ldg = 0.467, T_{app} = 5°C)

Table 4: Mass transfer mechanisms in strippers

Mole fraction units ($x10^5$) kmol/m^2-s	P = 30 kPa		P = 160 kPa	
	Rich End	Lean End	Rich End	Lean End
k_y'	1.5	3.7	22.8	37.7
K_y'	1.5	3.5	19.8	28.0
Gas Res. (%)	2	3	14	25
Kinetic Res. (%)	89	60	17	25
Diffusion Res. (%)	9	37	69	50

Task 2 – Pilot Plant Testing

Subtask 2.6 – Campaign 4

by Eric Chen

(Supported by EPA STAR Fellowship)

Introduction

In this reporting period, additional analysis was done on the data from Campaign 4. Work was begun on developing an Aspen absorber model from the potassium carbonate and piperazine VLE model developed by Hilliard (2005). Also, a literature review on absorber/stripper pilot plants and R&D policies of European and international organization was conducted in preparation for the GHGT-8 Conference in Trondheim, Norway.

Experimental – Pilot Plant

In the first campaign, it was erroneously concluded that the CO_2 calibration gas cylinders were based on a weight percent instead of volume percent. If it was assumed that the gases were weight percent, the material balance for the gas phase seemed to match the liquid phase. When the sale representative of the gas provider was initially consulted, we were informed that the cylinders were filled gravimetrically and the percentages were weight based. However, after the completion of the 4th campaign, the material balance did not seem to work when a weight based assumption was made. Further investigation into the matter and additional contact with the manufacturer indicated that the concentration were indeed volume percent and not mass. To further corroborate this, some of the cylinders were tested.

The CO_2 calibration gas verification experiments were conducted on a gas chromatography (GC) analyzer from the Freeman research group at the Pickle Research Center. The GC is normally calibrated using methane and carbon dioxide and therefore it was recognized that the results may slightly be off. The experiment was conducted by one of the members of the research group and the standard procedure was followed. The 12% and 16.9% CO_2 gas cylinders were tested. First, gas from the CO_2 cylinder was flowed to a mass flow controller and the volumetric flow was measured using a soap bubble flow meter. Next, the CO_2 gas was diluted with helium and the total gas flow was measured using the soap bubble flow meter. The gas mixture was then sent to the GC for analysis.

The results for the 12% and 16.9% were 13.2 mol% and 18.3 mol%, respectively. If a mass concentration was assumed for the gas cylinders, the concentrations would have been 8.3 mol% and 11.8 mol%. Since the results were much closer to the mole percent value, it was concluded that the cylinders were such. However, the correction of the CO_2 concentration implies that the gas rates for all of the campaigns were incorrect. It also implies that the gas rates or the liquid side material balance were not correct.

For the data analysis of Campaign 4, the CO_2 concentrations were converted to mole percent and the gas rate was reduced by 18.7% in order to make the material balance close (Figure 5). This was done only for the 5mK^+/2.5mPZ case and not for the 6.4mK^+/1.6mPZ case. This is because it appears that something else maybe be going on due to the vacuum stripping conditions.

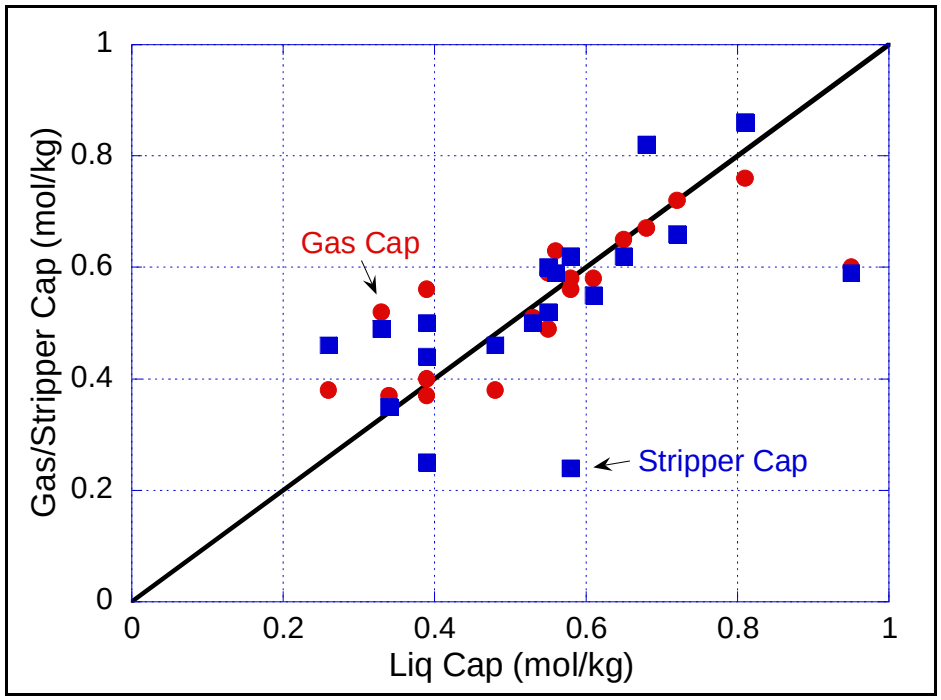

Figure 5: Corrected Material Balance for 5mK$^+$/2.5mPZ

With the corrected material balance, overall gas phase mass transfer coefficients (K_G) were calculated for the top, bottom, and overall beds of the absorber. The results are compared to bench-scale wetted wall column mass transfer coefficients (k_g') results at 60 ^oC. Figure 6 shows that the pilot plant results appear to be slightly lower than the bench-scale results. It is possible that there is some gas film resistance in the pilot absorber. However, based on initial calculations for k_l using the SRP Distill 2.0 program, the gas film resistance is approximately only 10%. It is possible that temperature affects and pinching in the column are contributing to the reduction in mass transfer performance.

Experimental – Aspen Plus

As part of the absorber modeling effort, work was undertaken to build an absorber model based on the Aspen Plus VLE model developed by Hilliard (2005). The absorber model was initially created using Ratefrac in Aspen Plus. However, the model would only converge at the low and high end ranges of lean loadings and did not converge over the lean loading range of the pilot plant. Also, the energy balance on the absorber did not work out. The temperature bulge did not exist and the temperatures profile of the absorber actually became colder than the entering gas and liquid streams (Figure 7).

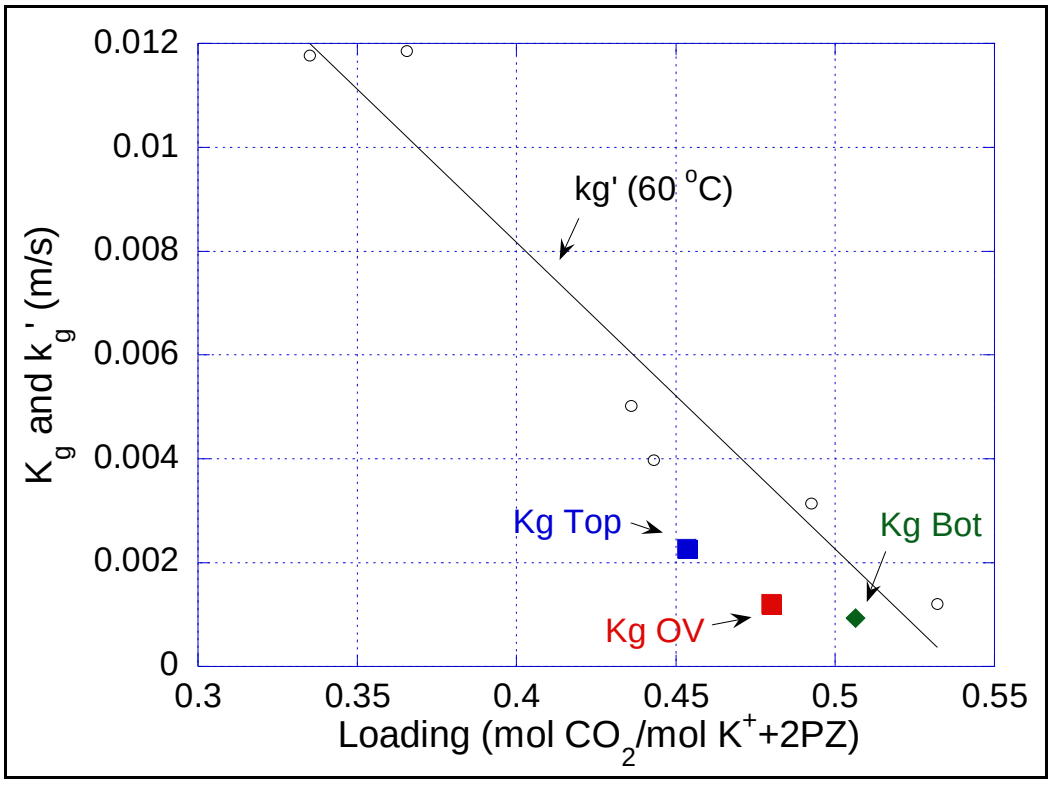

Figure 6: K_G and k_g' comparison from Campaign 4

Initially it was thought that the heats of formation for some of the species were incorrect. The following species required user input into Aspen for the heats of formation: PZH^+, $PZCOO^-$, $PZ(COO^-)_2$, and HPZCOO. For the HPZCOO ion species, the net charge is zero and was entered as such into Aspen. Therefore, it is possible that when Aspen performs an enthalpy balance, the species may not be recognized or causes Aspen to be confused. To partially test this theory, the HPZCOO species was deleted and appeared to give reasonable results for the temperature profile (Figure 8). Deleting the HPZCOO species is not a permanent solution. Therefore, we will continue to work on resolving the absorber model while incorporating the HPZCOO ion.

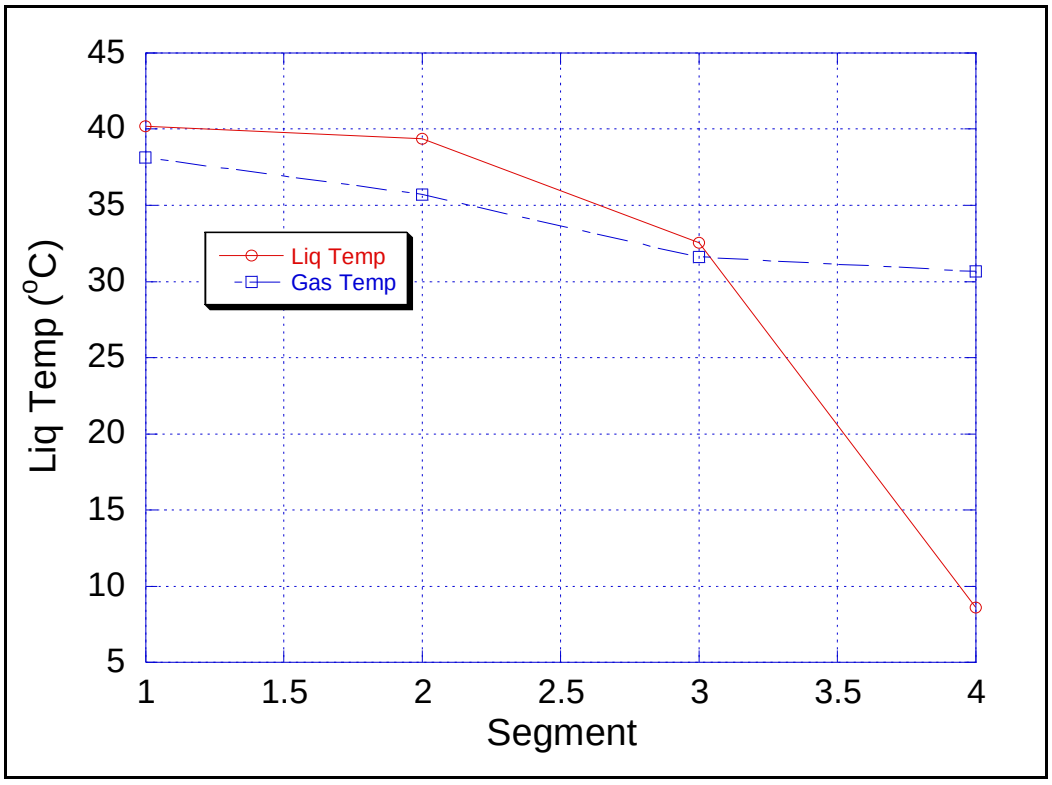

Figure 7: Temperature Profile Using Aspen Plus RateFrac Model with Hilliard VLE

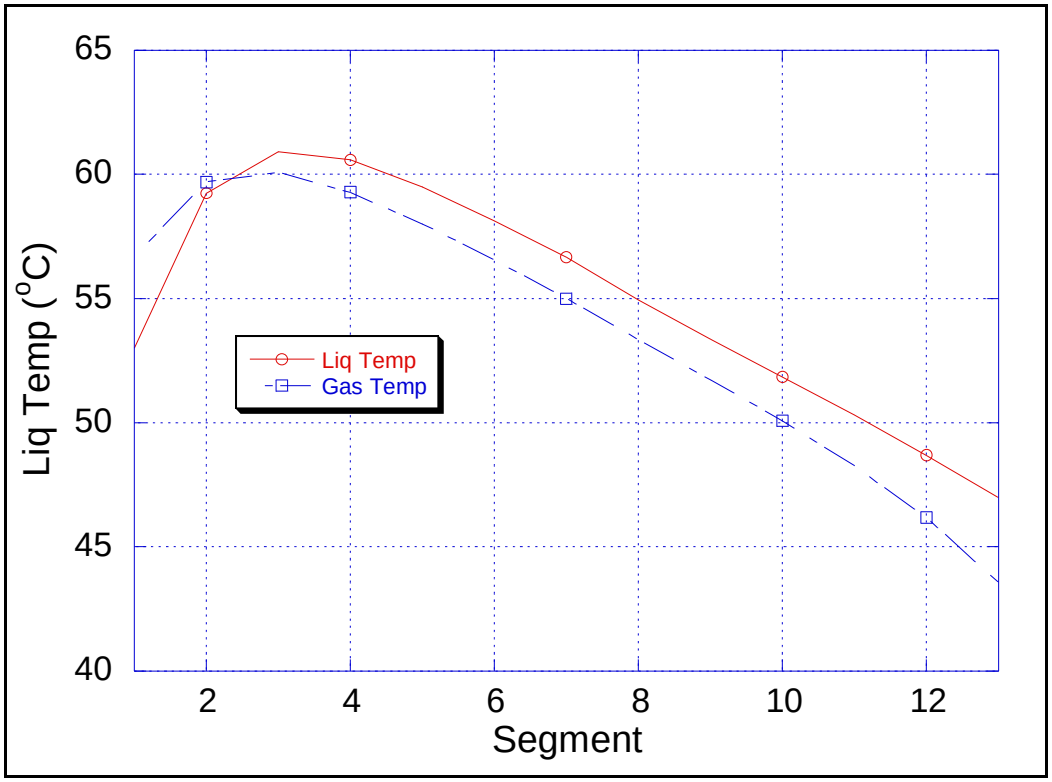

Figure 8: RateFrac Temperature Profile without $HPZCOO^-$ species

Some of the program files were sent to a specialist at Aspen. The Aspen specialist adjusted the heat of formation (DHAQFM) for PZH^+ and $PZCOO^-$ using trial and error and obtained reasonable heats of absorption. The heats of formation for the HPZ^+, $PZCOO^-$, $PZ(COO^-)_2$, and HPZCOO ions were re-evaluated and flash calculations were run with the Hilliard VLE model. However, when the heat of formation for the HPZCOO was changed, the heat of absorption did not change. The heat of formation for the HPZCOO was changed from -612283 KJ/kmol to 0 KJ/kmol and the heat duty for the flash calculation remained exactly the same. This indicates that there may be something incorrect with the HPZCOO species.

In the next phase of the absorber modeling, the HPZCOO species will be converted from an ion and into a molecule to see if this will resolve the problem. In order to do this, the chemical equilibrium constant for the equation containing the HPZCOO species will need to be converted using the activity coefficient at infinite dilution. Activity coefficients for the HPZCOO ion have been calculated and will be correlated to an equation and extrapolated to infinite dilution. The correlation will need to be dependent only on temperature. However, the activity coefficient is also dependent on loading and composition, which may complicate the conversion.

Conclusions and Future Work

The material balance for the $6.4mK^+/1.6mPZ$gas phase needs to be resolved. Once, the material balances have been rectified, K_G calculations will be made to quantify and compare the CO_2 absorption performances of the two solvents. Data from all three campaigns will also need to be reconciled.

The absorber model will continue to be modified. The purpose of the absorber model will be to validate the data obtained by the pilot plant. Once the model has been validated, it will be used to determine optimal operating conditions for the potassium carbonate and piperazine solvent.

Task 3 – Solvent Losses

Subtask 3.1 – Analysis of Degradation Products

Andrew Sexton

Supported by the Industrial Associates Program in CO_2 Capture

Introduction

This effort is an extension of work by George Goff on the oxidative degradation of MEA. Goff showed that oxidative degradation can be mass-transfer limited by the physical absorption of O_2 into the amine and not by reaction kinetics. Goff also theorized that the oxidative degradation of MEA produced volatile ammonia as well as a host of other proposed degradation products. The major degradation products among these include formic acid, acetic acid, oxalic acid, glycolic acid, nitrite, and nitrate.

The oxygen stoichiometry necessary to produce these degradation products varies for each individual component; overall, it varies anywhere from 0.5 to 2.5 (Goff, 2004). It is believed that the particular degradation products are specific to certain additives used to control corrosion in the absorption/stripping system – specifically iron and copper. For example, the following oxygen stoichiometries apply to the degradation of monoethanolamine:

$$MEA + 1.5\ O_2 \rightarrow 2\ Formate + Ammonia$$

$$MEA + 3.5\ O_2 \rightarrow 2\ Formate + Nitrate + Water$$

$$MEA + O_2 \rightarrow Glycolate + Ammonia$$

Goff's work on MEA degradation was limited to analyzing MEA degradation rates via the evolution of NH_3. The ammonia evolution rates were measured using a Fourier Transform Infrared (FT-IR) analyzer.

This effort will extend Goff's gas-phase analysis by applying various methods of liquid-phase analysis, specifically ion chromatography and nuclear magnetic resonance. These analytical methods will be used to quantify the rate of amine degradation as well as the rate of degradation product formation.

The oxidative degradation of the amines may significantly affect the economics and environmental impact of these solvent systems. Oxidative degradation results in fragmentation of the amine solvent. The identity and quantity of degradation products is required to assess their impact on the environment and the process economics and to design for corrosion prevention and solvent reclaiming.

Experimental

Ion chromatography is the most extensively used liquid-phase analytical method in this report. Anion chromatography utilizes a AS15 IonPac column made by Dionex (a low-capacity column designed to separate low-molecular weight anions, specifically acetate, glycolate, and formate). The column operates as a miniature adsorption tower. An unknown solution is injected into the column. An eluent of sodium hydroxide is continuously passed through the column to flush anions off the column and replenish it with hydroxide ions.

The ions leave the column and pass through a suppressor, which provides a steady supply of H^+ and OH^- ions. All cations are flushed out of the system as waste, leaving a weakly ionized solution of the unknown anion(s) in water. This solution is passed through a conductivity meter, which provides a signal peak with a specific height and area dependent upon the concentration of the anion in solution (Wang, 2005).

The most recent anion chromatography method analysis employs a linear gradient. The NaOH eluent starts at an initial concentration of 10 mM from time zero to eleven minutes. The weakly concentrated eluent is necessary to separate the low-molecular weight carboxylic acids, which tend to elute closely together. Once the low-MW compounds have eluted off the column, the method employs a linear gradient increasing from 10 to 45 mM NaOH from time eleven minutes to nineteen minutes. The eluent gradient stays constant at 45 mM until thirty minutes; the concentrated NaOH assists in eluting the more strongly retained anions from the column. Lastly, there is a step change back to the original eluent concentration of 10 mM to allow the system to re-equilibrate prior to injection of the next sample. The eluent flowrate stays constant at 1.60 mL/min, and the columns are operated at 30 ^oC.

The cation chromatograph operates in a similar manner. It utilizes a CS17 IonPac column manufactured by Dionex; it is a packed column that separates cations based on their affinity for the resin. The eluent is methanesulfonic acid, or MSA (CH_3SO_3H), and the suppressor flushes out all anions as waste. The end result is a weakly ionized solution of the unknown cation(s) in water (Dionex, 2005).

The method designed for degradation product analysis via cation chromatography uses a constant concentration of 13.5 mM MSA for thirty minutes. The eluent flowrate is 0.40 mL/min, and the columns are operated at 40 ^oC. When analyzing for amine concentrations, the concentration and flowrate are increased to 20 mM and 1.20 mL/min, respectively, for a time of five minutes.

Results

Using the most recently developed analytical methods for the AS15 and CS17 columns, the following degradation experiments were analyzed for degradation product formation rates:

1. March 2006 MEA experiment (Oxidative degradation of 7 m MEA, 55^oC, 1400 RPM, 0.2 mM Fe, 0.4 moles CO_2/mol MEA, 98%O_2/2%CO_2).
2. March/April 2006 PZ experiment (Oxidative degradation of 2.5 m piperazine/5 m $KHCO_3$, 55^oC, 1400 RPM, 500 ppm V^+, 98%O_2/2%CO_2).

An additional experiment was performed during the quarter, but it has not been analyzed completely:

1. April 2006 MEA/PZ experiment (Oxidative degradation of 7 m MEA/2 m PZ, 55^oC, 1400 RPM, 98%O_2/2%CO_2).

Furthermore, previous analyses for the following experiments were reanalyzed:

1. December 2004 MEA experiment (Oxidative degradation of 7 m MEA, 55^oC, 1400 RPM, 0.2 mM Cu, 0.4 moles CO_2/mol MEA, 98%O_2/2%CO_2).
2. September 2005 MEA experiment (Oxidative degradation of 7 m MEA, 55^oC, 1400 RPM, 0.2 mM Cu, 0.2 mM Fe, 0.4 moles CO_2/mol MEA, 98%O_2/2%CO_2).

3. November 2005 PZ experiment (Oxidative degradation of 2.5 m piperazine, 55°C, 1400 RPM, 500 ppm V^+, 98%O_2/2%CO_2).
4. January 2006 MEA experiment (Oxidative degradation of 7 m MEA, 55°C, 1400 RPM, 0.2 mM Cu, 0.2 mM Fe, 100 mM inhibitor A, 0.4 moles CO_2/mol MEA, 98%O_2/2%CO_2).

The amine solutions were oxidized for 12 to 14 days in a low-gas flow jacketed reactor at 55°C. The solutions were agitated at 1400 RPM to produce a high level of gas/liquid mass transfer by vortexing. 98% O_2/2% CO_2 at 100 ml/min is introduced across the vortexed surface of 350 ml of aqueous amine. Samples were taken from the reactor at regular intervals in order to determine how degradation products formed over the course of the experiment.

Figure 9 illustrates the concentration of significant degradation products from the oxidative degradation of 7 m MEA, as determined by anion chromatography, over a 12-day experiment in the low gas flow degradation apparatus. Samples were taken at five intervals during the course of the experiment. Anion chromatography shows that the most abundant degradation products are formate, nitrite, and nitrate. With the exception of glycolate, the rates of all degradation products are linear; the decreasing slope of the glycolate concentration shows that glycolate analysis may not be accurate.

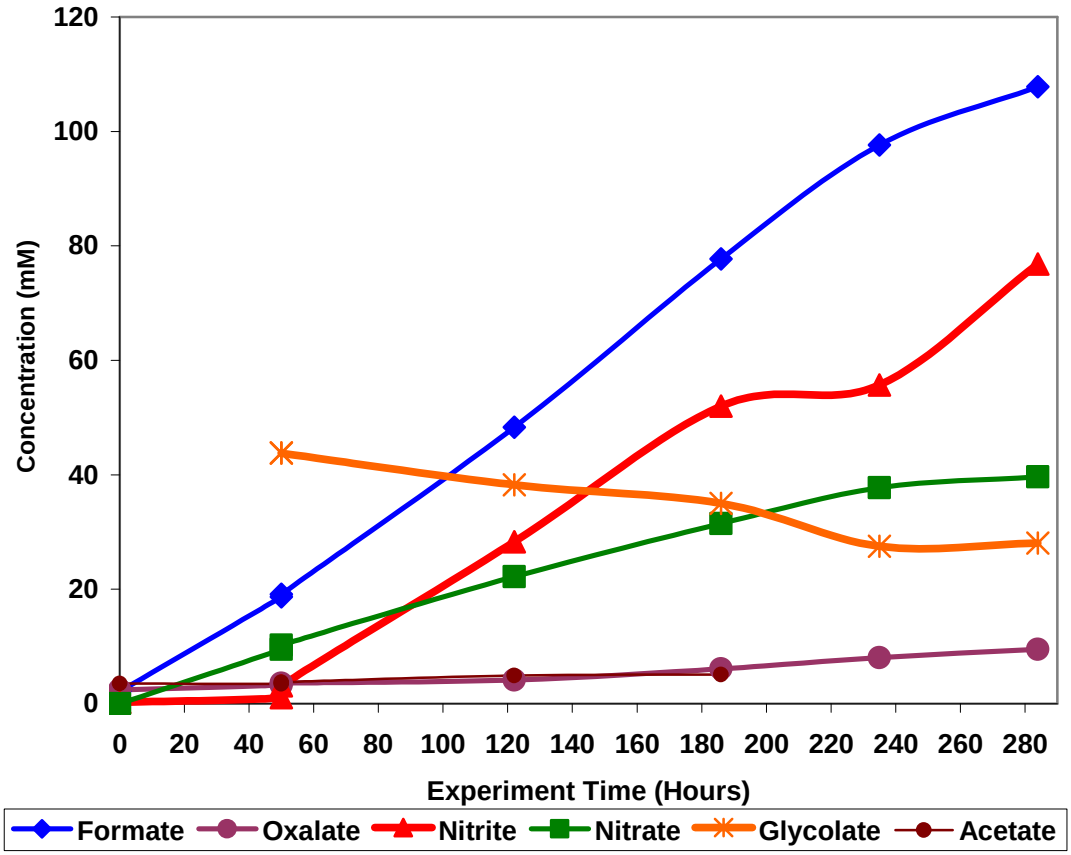

Figure 9: Oxidative degradation of 7 m MEA, 55°C, 1400 RPM, 0.2 mM Fe

In addition to the aforementioned products, a major anionic degradation product has yet to be identified. It was originally believed to be glycolate; however, it has been determined that

it is most likely glyoxylic acid. Figure 10 shows a plot of the raw peak areas versus time for all degradation products. This figure shows that the unidentified degradation product is on the same order of magnitude of formate and needs to be positively identified.

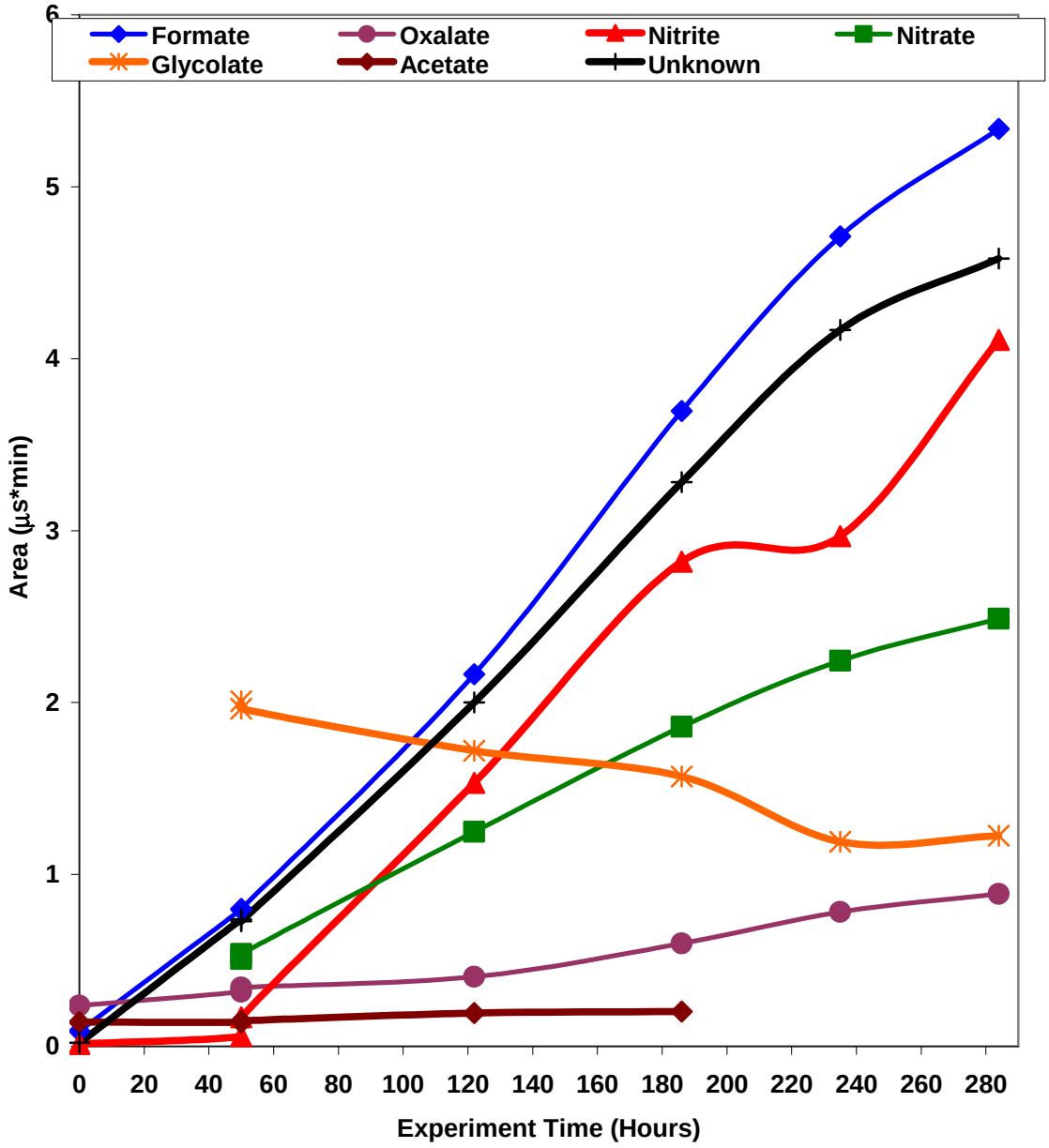

Figure 10: Oxidative degradation of 7 m MEA, 55°C, 1400 RPM, 0.2 mM Fe

Figures 11 and 12 show revised graphs of the formation of degradation products from MEA and piperazine. Figure 11 depicts illustrates the formation of degradation products from MEA in the presence of copper. Analysis shows that glyoxylate (not yet confirmed) is just as an important degradation product as formate in the oxidative degradation of MEA – for both iron and copper systems. Acetate and glycolate are present as degradation products; however, they aren't shown on the graph because of inconsistencies in the intermediate samples.

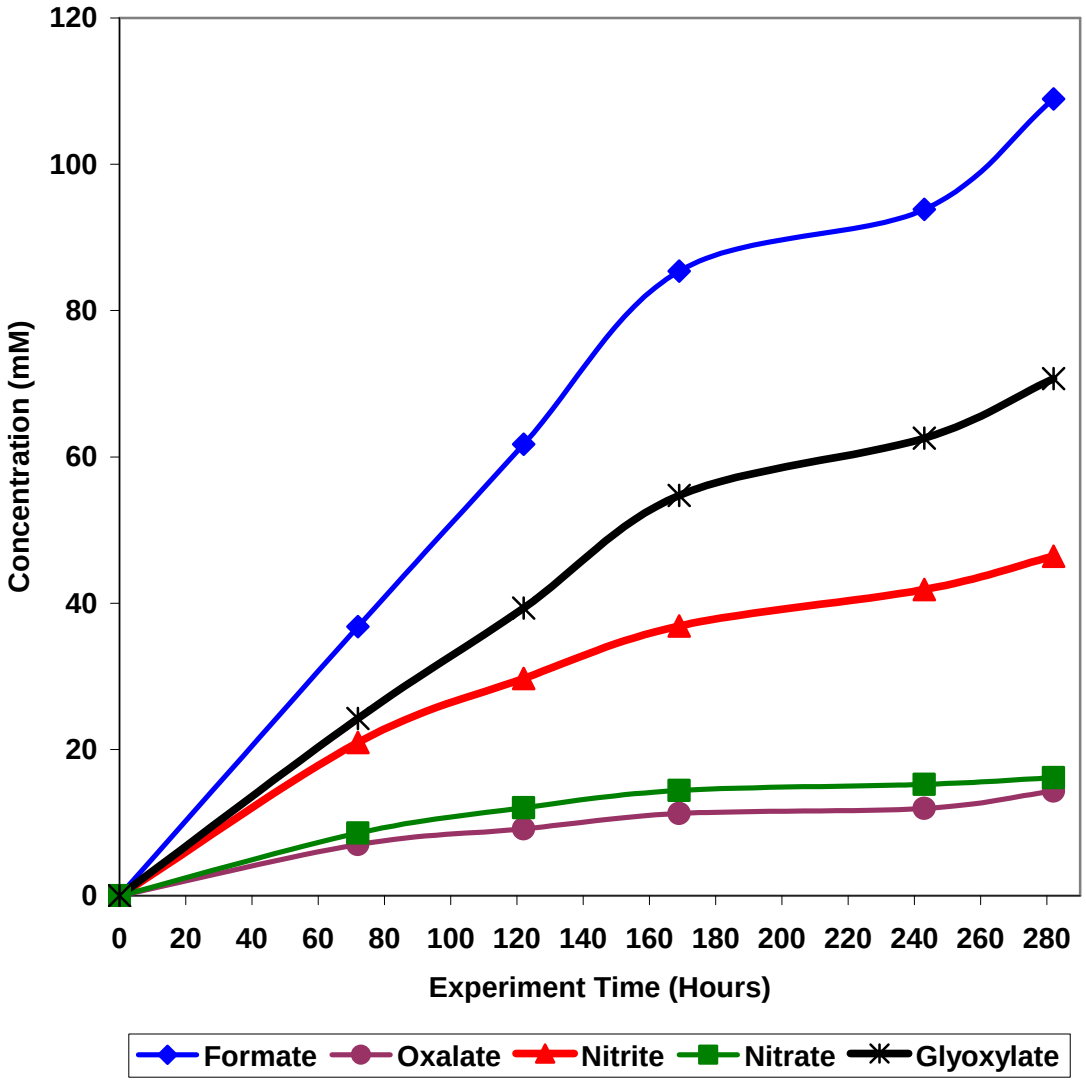
120
100
80
60
40
20
0
Concentration (mM)
0
20
40
60
80
100
120
140
160
180
200
220
240
260
280
Experiment Time (Hours)
Formate
Oxalate
Nitrite
Nitrate
Glyoxylate

Figure 11: Oxidative degradation of 7 m MEA, 0.2 mM Cu, 55°C, 1400 RPM

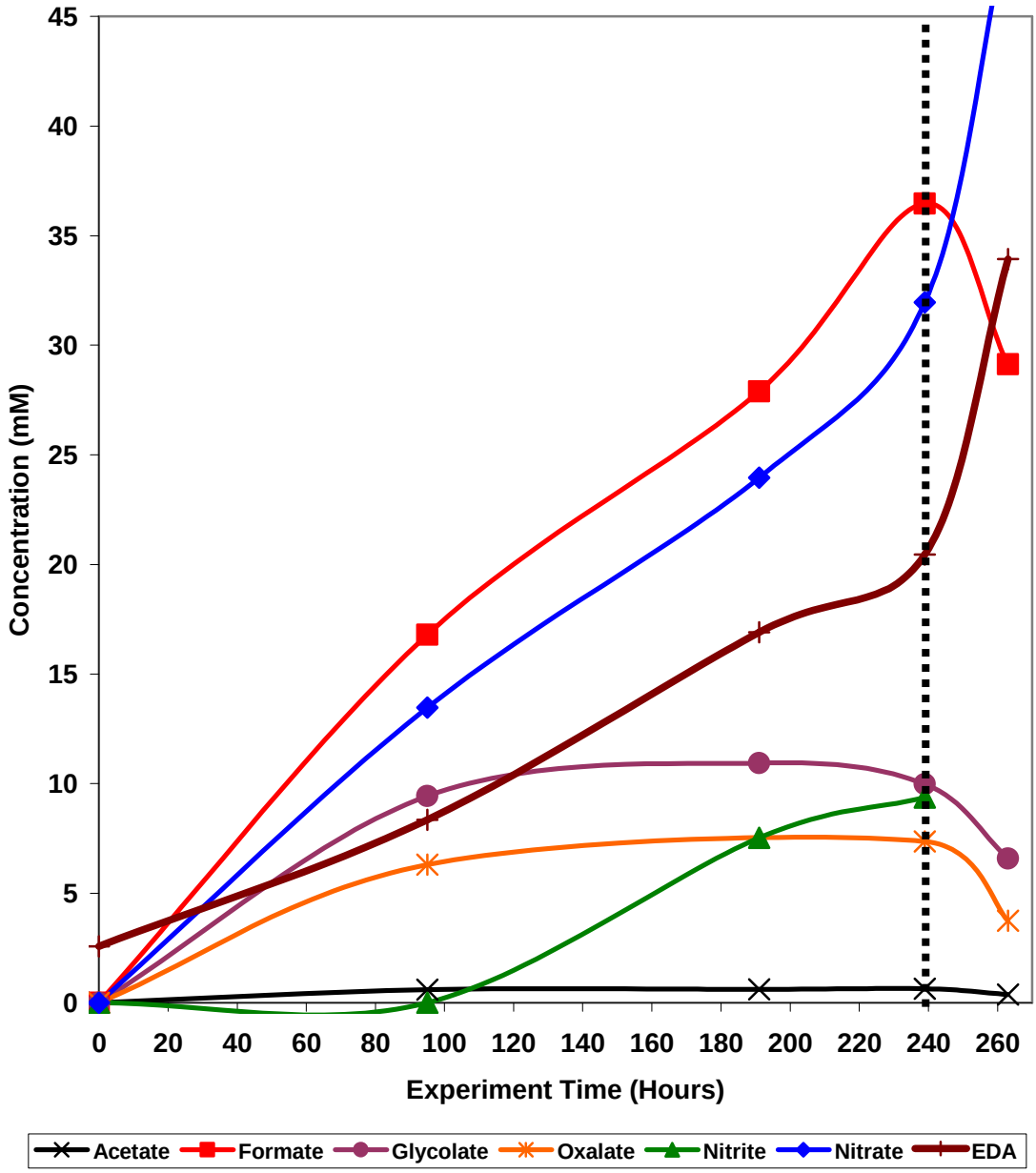

Figure 12: Oxidative degradation of 2.5 m Pz, 500 ppm V^{+}, 55°C, 1400 RPM

Figure 12 revisits the degradation of 2.5 molal piperazine in the presence of vanadium, commonly used as a corrosion inhibitor in piperazine systems. Not included on the graph are the two unknown cationic degradation products mentioned in previous progress reports, which combined were shown to be approximately half the amount of ethylenediamine.

Tables 5 and 6 summarize degradation rates (in mM/hr) for piperazine and monoethanolamine degradation experiments. Table 5 summarizes the change in stoichiometry and product formation by changing degradation catalysts added to the system; Table 6 notes the differences between MEA degradation (when a degradation inhibitor is added to the system) and

piperazine degradation. The row labelled “carbon” in Table 5 is the sum of carbon atoms from all the carbon-containing degradation products (the carboxylic acid degradation products from MEA).

Table 5: Summary of MEA Degradation Product Formation Rates in mM/hr

Distinguishing Conditions	0.2 mM Fe	0.2 mM Cu	0.2 mM Cu and Fe
Formate	0.40	0.39	0.67
Glycolate	0.10	0.13	0.02
Acetate	0.02	0.01	0.02
Oxalate	0.04	0.04	0.05
Nitrate	0.15	0.05	0.14
Nitrite	0.31	0.16	0.19
Carbon	0.73	0.75	0.85

Table 6: Summary of Degradation Product Formation Rates in mM/hr

Distinguishing Conditions	0.2 mM Cu and Fe, 100 mM "A"	2.5 m Pz, 500 ppm V+	5 m K+/2.5 m Pz, 500 ppm V+
Formate	0.04	0.18	<0.01
Glycolate	0.12	0.03	0.01
Acetate	0.02	<0.01	0.01
Oxalate	0.01	0.04	<0.01
Nitrate	<0.01	0.19	<0.01
Nitrite	0.03	<0.01	<0.01
EDA		0.09	

Conclusions and Future Work

The four carboxylic acids have been identified as reaction products of amine degradation, confirming the finding in the Dow Rooney paper. In addition, nitrite, nitrate, and ethylenediamine have been discovered as significant amine degradation products. Based on the most recent ion chromatography analysis, formate and an unknown carboxylic acid (likely glyoxylate) are the most abundant products of the oxidative degradation of monoethanolamine.

Carboxylic acid degradation rates are similar between iron and copper-added MEA systems. However, iron-added systems favor the formation of nitrate and nitrite more than copper-added systems. This conclusion supports Goff’s findings, which showed a higher ammonia formation for copper-added MEA systems versus iron systems. Furthermore, a combination of iron and copper shifts degradation product formation from glycolate towards formate.

When inhibitor A is present in 7 m MEA in the presence of copper and iron, oxidative degradation is reduced greatly (by approximately 70% as compared to systems without inhibitor A). Glycolate is the most prevalent degradation product when inhibitor A is present, but it is in a much smaller quantity than the most abundant product in other MEA experiments. From this analysis, one can conclude that inhibitor A does an excellent job at slowing down the rate of MEA degradation.

When inhibitor A is not present, the rate of piperazine oxidative degradation is much slower than the rate of MEA degradation. Ethylenediamine is a degradation product specific to piperazine. There is also a shift in the type of degradation products. When MEA is degraded, the carboxylic acid degradation products appear in greater quantities than nitrogen-containing products (nitrite, nitrate, and EDA). On the other hand when piperazine is degraded, the opposite is true.

The addition of 5 molal K^+ to piperazine systems effectively prevents piperazine degradation. This is because K^+ reduces O_2 solubility in the amine. Currently, a degraded MEA/piperazine blend is being analyzed to determine which one degrades faster when they are used in conjunction with one another.

There are still some issues to resolve regarding the IC analysis. One important anionic degradation product and two cationic degradation products remain unidentified. Glyoxylate, methylamine, ethylamine, and ammonia are the most likely candidates. Quantifying these degradation products and understanding oxidation chemistry will improve the environmental, process, and economic value of the CO_2 removal system.

Subtask 3.1a – Nitrosamines

by Andrew Sexton

(Supported by the Industrial Associates Program in CO_2 Capture)

Recent ion chromatography analysis has revealed nitrite and nitrate as major oxidative degradation products of monoethanolamine, and more importantly, piperazine. If nitrates – and nitrites especially – are present in substantial quantities in piperazine solution, it is possible that nitrite (or some other type of nitrogen compound) could react with piperazine to form a class of compounds known as nitrosamines.

In the pilot plant located at the Pickle Research Center, CO_2 capture is simulated by an absorption/stripping system by which CO_2 is removed from a synthetic flue gas using an amine solvent. One amine solvent is an aqueous solution of 2.5 molal piperazine promoted by 5 molal of K^+ ion (in the form of potassium carbonate/bicarbonate). Oxidative degradation takes place in the middle of the absorber, and has been confirmed using anion and cation analysis. Therefore, nitrosamine formation from the oxidative degradation of piperazine solvent is a legitimate concern in the post-combustion removal of CO_2.

Toxicological studies have shown that piperazine can nitrosate to form *N*-mononitrosopiperazine (MNPz) and *N, N'*-dinitrosopiperazine (DNPz) in animals in vitro (Tricker et al., 1991). The formation of these compounds can come about by exposure to both nitrites and piperazine in the body. MNPz has been reported to be non-carcinogenic in rats (Love et al., 1977); conversely, the fact that significant levels of its carcinogenic metabolite

NHPYR (Nitroso-3-hyrdoxypyrrolidine) can be detected in urine provides ample justification of the limited use of piperazine in medicine. Unlike its precursor, DNPz is both mutagenic and carcinogenic in experimental animals (Elespuru and Lijinsky, 1976).

Under in vitro conditions (1 mM of piperazine with 2 mM sodium nitrite in 1 M citrate/HCl buffer) at 37 ^{o}C, piperazine nitrosated to form MNPz and DNPz over the range of pH 0.5 to 5.5. At pH maxima of 3.0, a 51% yield of MNPz and 3.8% yield of DNPz were obtained, corresponding to a 9.3% yield of DNPz from MNPz. Nitrosamine concentrations were determined using a gas chromatograph with a thermal energy analyzer (Dawson and Lawrence, 1986).

In general, carcinogenous nitrosamines may be produced by the reactions of NO_x and secondary amines. Nitrosamines prepared from primary amines degrade at less than room temperature (Challis and Challis, 1982). Tertiary amines do not directly form stable nitrosamines, but they can react with NO_x to produce secondary nitrosamines. Tertiary amines react with aqueous nitrous acid, contrary to common belief, and undergo dealkylation to form a carbonyl compound, a secondary nitrosamine, and nitrous oxide (Smith and Loeppky, 1967).

The most probable mechanism is reaction of NO with an aminium radical or radical ion formed by amine oxidation with a free radical. This mechanism requires that the amine be in the process of oxidizing and that there be a sufficient concentration of NO in the solution. NO is not very soluble and would not be readily absorbed in an aqueous solution. It is present in low concentration in the flue gas, in contrast to percent or higher levels in studies by organic chemicals that produce nitrosamines (Challis and Challis, 1982).

$R_2N^{\cdot} + NO \rightarrow R_2N\text{-}NO$

The gases N_2O_3 and N_2O_4 are effective reactants for making nitrosamines (Lovejoy and Vasper, 1968). Kinetic studies of both diazotization (conversion of an aromatic primary amine into a diazonium compound) and deamination (removal of an NH group from an amino compound) in dilute solutions have given the equation rate = k [amine] $[HNO_2]^2$. Similarly, the combination of air and NO results in quick conversion of secondary amines to nitrosamines (Challis and Kyrtopoulos, 1979), probably by oxidation of NO to N_2O_3. However, concentration of N_2O_3 and the oxidation of NO are both second order or higher processes. At the low concentrations of NO_x in the flue gas there is very little N_2O_3 and very little opportunity for oxidizing NO to NO_2.

Both N_2O_4 and N_2O_3 reacted with aqueous piperidine (similar in structure to piperazine) in aqueous 0.1M NaOH give substantial amounts of *N*-nitrosopiperidine, plus smaller amounts of *N*-nitropiperidine in the case of N_2O_4. All these reactions are considered to occur predominantly in the aqueous phase and to be complete in a few seconds. With excess amine, yields of *N*-nitrosopiperidine reach maximum values. The dependence of product yields suggests that *N*-nitrosopiperidine formation follows Rate = k_p [piperidine] $[N_2O_x]$. Formation of *N*-nitrosopiperidine from the gaseous reactants occurs predominantly in the gas phase. N_2O_3 is nominally 3.3 times more reactive than N_2O_4 towards piperidine (Challis and Kyrtopoulos, 1979).

A pH of 2 to 5 is required for the production of nitrosamines from nitrite, where some free amine is left and HNO_2 can decompose to the active reagent N_2O_3. Nitrosamine formation is generally presumed to require acidic conditions (pH < 5) where nitrite is converted to nitrous

acid and H_2ONO^+ (nitrous acidium ion) exists at low concentration. With one or two exceptions, nitrosation appears to involve the unprotonated amine and a reagent such as N_2O_3, NOCl, H_2ONO^+, or NO^+ existing in equilibrium with both HNO_2 and NO_2^-. These reactions appear to be encounter-controlled and therefore very rapid. The oxidation of NO to a more reactive entity brought about by slow diffusion of air into the reaction vessel appears to be the rate-limiting process (Challis and Challis, 1982).

While the above papers provide insight into nitrosamines, they do not apply to pilot plant conditions because the absorber and stripper are run at basic pH. On the other hand, Keefer and Roller (1973) have shown that formaldehyde will catalyze the reaction of nitrite and diethylamine at pH 6.4 - 11 to produce diethylnitrosamine. The paper postulates that the nitrite reacts with the iminium salt produced by the interaction of the aldehyde and the secondary amine. Yield is almost independent of hydrogen ion concentration in basic medium, the quantity of product at pH 11.0 being 40 percent of that found at pH 7.5.

Piperidine, similar in structure to piperazine, has shown to be one of the most reactive secondary amines. In the absence of formaldehyde, no nitrosamine could be detected above pH 7.5 under these conditions. Any nitrite present in the system could generate nitrosamines by this mechanism. This study is important because formaldehyde has been hypothesized as an intermediate degradation product in the oxidative degradation of amines.

Calle et al. (1992) studied the nitrosation of sixteen secondary amines by nitropropane (PrONO) and nitrobutane (BuONO) in a strongly alkaline medium (0.10 M NaOH with sodium perchlorate) – including piperazine. Nitrites were not formed in the actual bulk of the reaction medium, but rather isolated, purified and used in pure form. The following rate equations were determined

$$\text{Rate} = k_{2obs} [\text{amine}] [\text{nitrite}]$$

$$\text{Rate} = k_2 [\text{amine}] [\text{nitrite}] / (1 + [H^+]/K_a) \text{ where } [H^+] << K_a$$

In another experimental study, the vapor pressures of 30 *N*-nitrosamines were calculated between the temperatures of 0 and 40^{o}C using the Hass/Newton equation (Klein, 1982):

$$\Delta t = (273.1 + t) (\log 760 - \log p)/ \phi + 0.15 (\log 760 - \log p)$$

$\Delta t = {}^oC$ to be added to the temperature at the observed pressure to yield the boiling point at 760 mmHg

$t = {}^oC$ temperature determined at pressure p

$\log p = \log_{10}$ of the observed pressure in mmHg

ϕ = the entropy of vaporization at 760 mmHg (a function of temperature and structure)

Based upon these calculations, pure nitrosopiperidine (very similar in structure to mononitrosopiperazine) has a vapor pressure of 0.44 mmHg at 40 ^{o}C (or 580 ppm in air at saturation). For three of the thirty nitrosamines, the vapor pressure of pure compounds were obtained by gas phase analysis from the saturated atmosphere above a layer of nitrosamine. Experimental results were determined to be within 10 % of the calculated values. In conclusion,

the volatility of nitrosamines is not insignificant; it cannot be excluded that if nitrosamines are being formed, they are somewhat volatile and their vapors could be inhaled (Klein, 1982).

There are basic conditions at which nitrosamine formation can be prevented. U.S. Patent No. 5,223,644 (Blezard and Jones, 1993) proposed to use bicarbonates and/or carbonates to inhibit the formation of nitrosamines during the preparation, storage, and/or use of amine oxides. Amine oxides are conventionally prepared by reacting a tertiary amine with hydrogen peroxide; sodium bicarbonate (usually below 1% by weight) is used to catalyze this reaction. This patent proposes to use 2.5% to 20% by weight of a bicarbonate/carbonate stabilizer to inhibit nitrosamine formation (a by-product of amine oxide production) below levels of 100 parts per billion (ppb).

Although this process was proposed for tertiary amines, *N*-substituted piperazines may be treated by this process as well. Previously, temperature rise was a significant problem in the formation of amine oxides; the bicarbonate/carbonate stabilizer renders the solution heat resistant with respect to the formation of nitrosamine impurities. Total nitrosamine contents were determined as total NO by a chemiluminescence method, whereby the sample, after destruction of nitrite ions by sulphuric acid, is denitrosated and the NO gas liberated therefrom is fed into a chemiluminescence analyzer (Blezard and Jones, 1993).

Similarly, Kirsch et al. (2000) performed experiments using bicarbonate ion to inhibit nitrosamine formation by carbamate formation. Both morpholine and piperazine were tested; since the formation of an amine carbamate depends on the pK_a value of the corresponding ammonium ion, experiments with piperazine [$pK_{a1} = 5.55$] were carried out at pH 7.4. At a concentration of 1 mM piperazine with 25 mM $HCO3^-$, nothing was detected via ^{13}C NMR. However at a concentration of 2 mM piperazine, formation of piperazine carbamate is evident. The concentration of piperazine carbamate increases with increasing piperazine concentrations, until at 100 mM all of the applied $^{13}CO_2$ is completely converted.

To further demonstrate that formation of piperazine carbamate is responsible for the depleted yield of nitrosopiperazine, additional experiments with piperazine (2 mM) and various concentrations of $HCO3^-$ were performed at pH 7.4. In the presence of 200 mM $HCO3^-$, *N*-nitrosation of piperazine (2mM) was inhibited by about 66% (from 300 μM nitrosopiperazine in the absence of $HCO3^-$ to 115 μM at 200 mM $HCO3^-$).

$NaNO_3$ was used in control experiments as an additive to show that alterations in the ionic strength cannot induce a decrease in the yield of nitrosopiperazine. When the $HCO3^-$ concentration is increased from 50 to 200 mM, piperazine carbamate concentration doubled and nitrosopiperazine concentration was halved. This leads to the conclusion that piperazine carbamate formation is most likely responsible for the diminished yield of nitrosopiperazine (Kirsch et al., 2000).

Although formaldehyde is likely present in basic conditions in the absorber/stripper system, the presence of potassium carbonate should prevent the formation of nitrosamines by the formation of carbamates – which can be confirmed by NMR analysis. Furthermore, MNPz is an unstable compound and the formation reaction can be reversed back to piperazine and nitrate. The major uncertainty involves the concentration of piperazine; most studies involve dilute quantities of all the reactants involved, while the pilot plant uses 30% by weight piperazine.

Subtask 3.3 – Thermal Degradation

Jason Davis

(Supported by this contract)

Introduction

This subtask will be used to define future work for the development of a kinetic model for MEA thermal degradation. While the products of thermal degradation have been identified, the kinetics of the thermal degradation pathways have not been clearly defined. Currently, the concentrations of MEA are capped at 30 wt% to minimize thermal degradation and prevent corrosion in industrial applications; however, with a better understanding of degradation kinetics, this number can be optimized. This work will also allow us to better understand solvent losses by thermal degradation.

Theory

Talzi (2003) describes the mechanisms for thermal degradation and uses NMR to characterize the degraded solutions. In CO_2 capture, MEA associates with CO_2 in the absorber to form MEA carbamate as illustrated below.

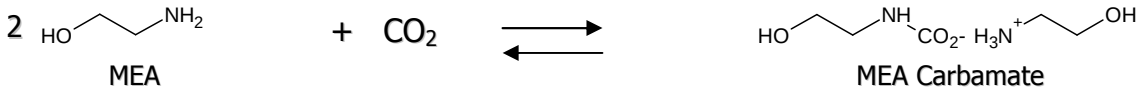

This reaction is normally reversed in the stripper, but in some cases the MEA carbamate will polymerize to form 2-oxazolidone, which is also a reversible reaction, as shown below.

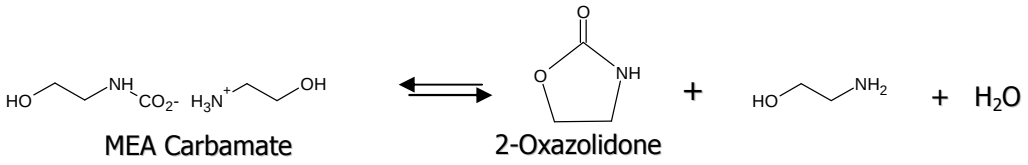

MEA carbamate can also irreversibly dehydrolize to form N,N'-di(2-hydroxyethyl)urea.

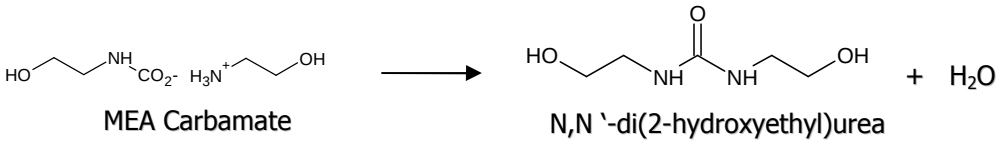

The former product, 2-Oxazolidone, can then react with another molecule of MEA to form 1-(2-hydroxyethyl)-2-imidazolidone which is sometimes referred to as HEIA.

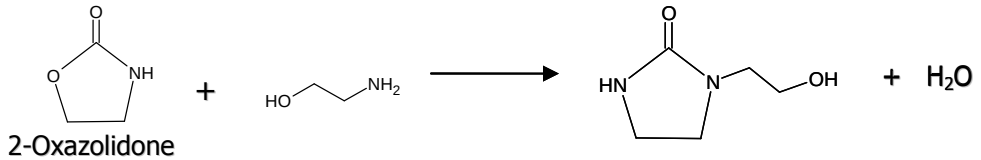

2-Oxazolidone

1-(2-hydroxyethyl)-2-imidazolidone

(HEIA)

HEIA can then be hydrolyzed to form N-(2-hydroxyethyl)-ethylenediamine or HEEDA.

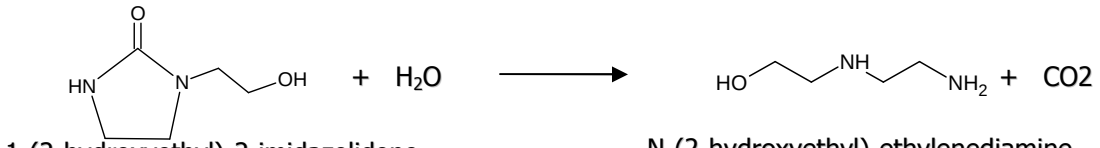

1-(2-hydroxyethyl)-2-imidazolidone

(HEIA)

N-(2-hydroxyethyl)-ethylenediamine

(HEEDA)

These four species (2-oxazolidone, dihydroxyethylurea, HEIA and HEEDA) are believed to be the main products of thermal degradation. The rate of formation of these products is a function of temperature (faster kinetics), CO_2 loading (more carbamate present) and MEA concentration.

Current and Future Work

A set of 5-10ml sample bombs are being constructed and will be filled with C^{13} labeled CO_2 rich amine solutions and placed in a temperature controlled oven. The temperature and pressure of each bomb will be recorded and the samples will be analyzed by NMR initially to help define what degradation products are present and their relative quantity. In the future, a 500cc Zipperclave from Autoclave Engineers will also be used to control the temperature and pressure of a batch of MEA loaded with CO_2. The temperature, loading, and MEA concentration will be varied and the resulting liquid will be analyzed by a yet to be developed HPLC method and previously developed GC method from the University of Regina.

Subtask 3.4 – Amine Volatility

by Marcus Hilliard

(Supported by the Industrial Associates Program)

Reagents

Sample solutions containing ultra-pure deionized water (H_2O) were obtained from the Department of Chemical Engineering at The University of Texas at Austin without further purification. Nitrogen (N_2) gas was obtained from the Cryogenics Laboratory at The University of Texas at Austin at a purity of 99.0 mol%.

Experimental Methods

Tests were conducted in the stirred reactor system, documented in a previous report, using ultra-pure deionized water as an initial baseline to assess the amount of error in the experimental method as shown in Figure 13.

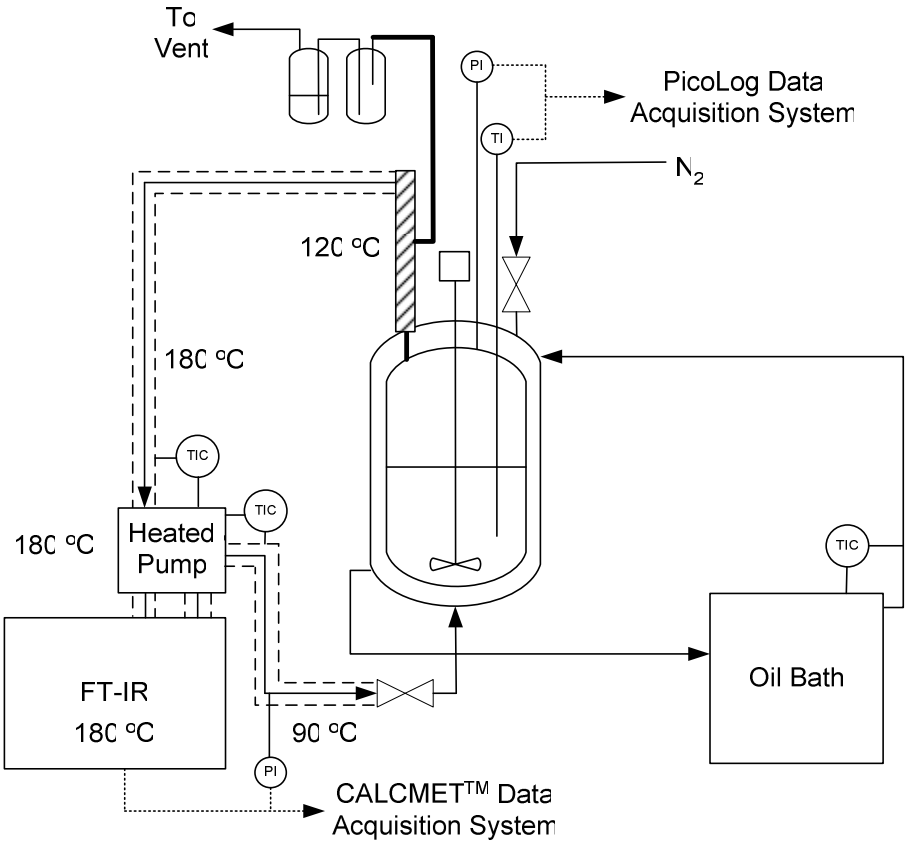

Figure 13: Process Flow Diagram for Vapor Phase Speciation Experiments.

These tests focused on the agitation rate and the return vapor temperature to the reactor. The actual pure component vapor pressure (P_{H2O}^{act}) was calculated using the DIPPR model where the equation is listed below:

$$P_{H2O}^{act} = \exp\left(73.649 - \frac{7258.2}{T} - 7.3037 \ln T + 0.0000041653 T^2\right) \qquad (1)$$

where the resulting vapor pressure is given in Pa and the temperature is in K. During the experiment equilibrium was obtained when the temperature in the reactor and the H_2O concentration in the vapor phase were constant.

During an experiment, the temperature of the reactor is a function of the water bath and heated line set points and heat losses to the environment. The reactor has been wrapped in insulation to reduce heat losses and to maintain a constant reactor temperature. A section of piping between

the heated line and inlet to the reactor was not insulated due to working conditions of the experiment. Thus, the vapor stream is allowed to contact ambient air and possibly allow condensation to occur. The following design matrix, Table 7, outlined the conditions that were used for these tests. All previous experiments were conducted with an agitation rate of 350 rpm and a heated line set point of 90 ^{o}C. The agitation rate was chosen to avoid the solution splashing the walls of the reactor and thus liquid entrainment into the vapor phase.

Table 7. Design Matrix for H_2O Benchmark.

Agitation rate: 350 RPM

T_{WB}	T_{HL}	T_{HL}-T_{WB}
35	90	55
45	90	45
55	90	35
65	90	25
35	90	55
45	100	55
55	110	55
65	120	55

where T_{WB} and T_{HL} are the water bath and heated line set points, respectively.

Based on the above design matrix, the following results were obtained as shown in Table 8.

Table 8. Experimental Results for H_2O via FTIR Analysis.

Date	T_{rxn} (^{o}C)	y_{H2O}	P_{rxn} (kPa)	P_{H2O}^{exp} (kPa)	P_{H2O}^{act} (kPa)	Error (%)	Exp/Est	RPM	HL (^{o}C)	WB (^{o}C)	HL-Rxn	HL-WB
3/31/2006	36.01	0.0623	100.2	6.2	6.0	-4.84	1.048	350	90	35	53.99	55
3/31/2006	44.07	0.0963	100.0	9.6	9.1	-5.29	1.053	350	90	45	45.93	45
3/31/2006	53.05	0.1421	100.0	14.2	14.3	0.98	0.990	350	90	55	36.95	35
5/23/2006	34.99	0.0604	100.1	6.0	5.6	-7.47	1.075	350	90	35	55.01	55
5/23/2006	43.32	0.0942	100.0	9.4	8.8	-7.09	1.071	350	90	45	46.68	45
5/23/2006	51.76	0.1387	99.9	13.9	13.5	-2.86	1.029	350	90	55	38.24	35
5/24/2006	35.12	0.0597	100.1	6.0	5.7	-5.43	1.054	350	90	35	54.88	55
5/24/2006	44.28	0.0935	100.1	9.4	9.2	-1.19	1.012	350	100	45	55.72	55
5/24/2006	52.59	0.1394	100.0	13.9	14.0	0.67	0.993	350	110	55	57.41	55
5/24/2006	60.97	0.205	99.8	20.5	20.9	1.90	0.981	350	120	65	59.03	55

From the above results we could calculate the correct temperature based on the measured partial pressure of H_2O from Equation 1 as shown in Table 9.

Table 9. Comparison between calculated and measured reactor temperature at the measured partial pressure of H_2O.

Date	T_{rxn} (^oC)	T_{DIPPR} (^oC)	Error (%)
3/31/2006	36.01	36.88	2.34
3/31/2006	44.07	45.07	2.22
3/31/2006	53.05	52.85	0.38
5/23/2006	34.99	36.30	3.61
5/23/2006	43.32	44.64	2.96
5/23/2006	51.76	52.34	1.10
5/24/2006	35.12	36.08	2.66
5/24/2006	44.28	44.51	0.52
5/24/2006	52.59	52.45	0.26
5/24/2006	60.97	60.56	0.69

For a single component system, the composition of the vapor is the dew point at a given temperature. We can see that at a given partial pressure of H_2O that the temperature in the reactor is lower than the dew point due to condensation in the non-insulated section of piping and to a low mass transfer rate, vis-à-vis agitation rate of the reactor as shown in Figure 14.

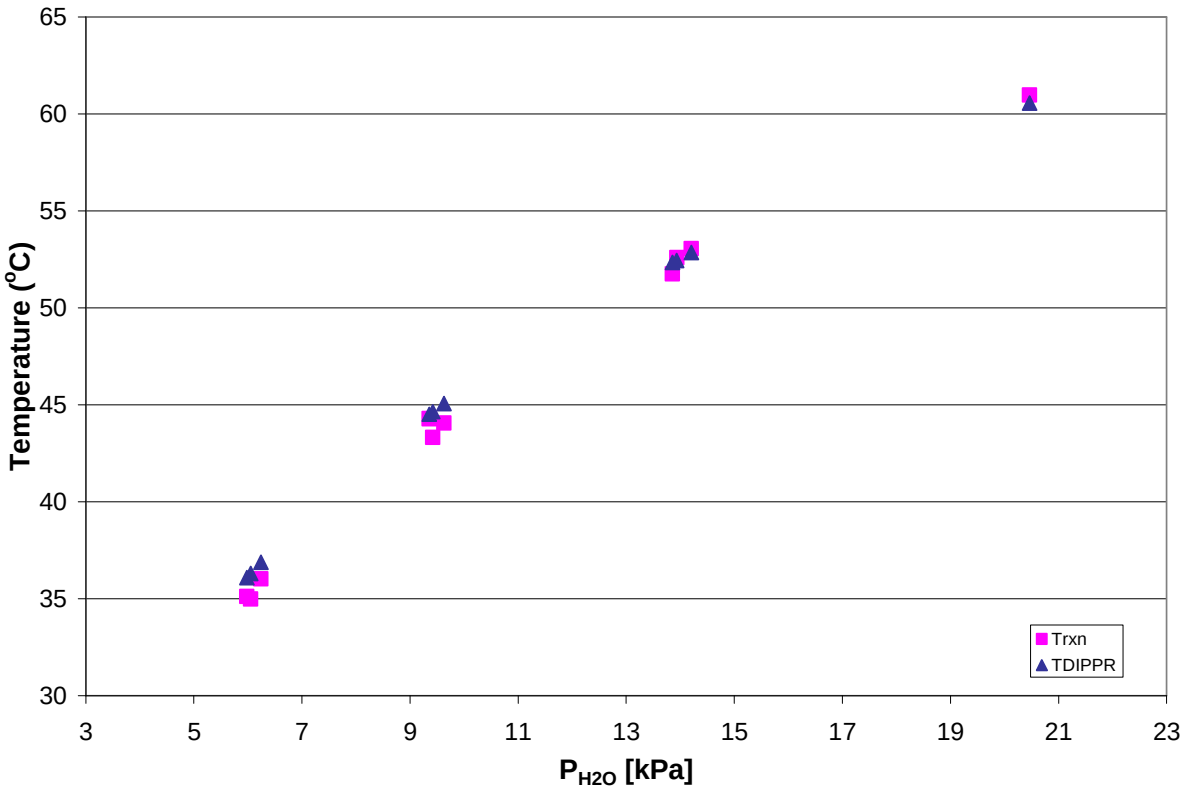

Figure 14: Effect of vapor condensation on the reactor temperature.

We know that the temperature of the reactor is a function of the water bath and heated line set points and heat losses to the environment. So we can see if varying the heated line set point would allow the vapor time not to condense in the non-insulated section. Figure 15 shows the difference between the heated line set point and the temperature in the reactor versus the error in

the H_2O partial pressure measurement. For three cases, we were able to isolate the vapor stream above/below the dew point. For the ♦ points, observations during the experiment noted that the vapor stream was condensing before the reactor; where as for the ▲ points, observations during the experiment noted that the vapor stream was entering the reactor at a saturated condition.

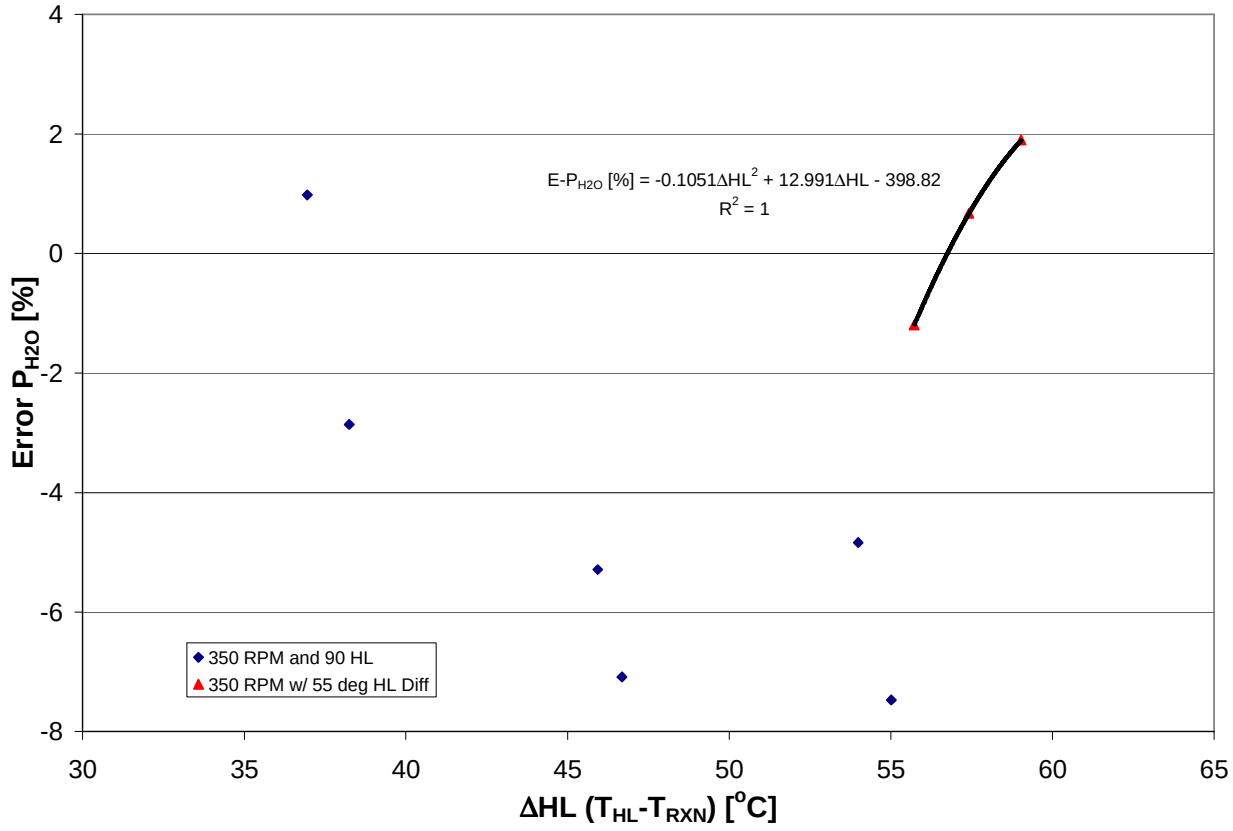

Figure 15: Error associated with each experiment in terms of the difference between the heated line set point and the reactor temperature.

For future experiments, we will be able to adjust the heated line set point to allow the vapor stream to enter the reactor at a saturated condition. For previous experiments, we were able to correlate the reactor temperature versus the correct temperature as shown in Figure 14 to correct previous experiments for the effect of pre-condensation of the vapor stream given by the following equation.

$$T_{corr}\left[^{o}\mathrm{C}\right] = -0.0073T_{\exp}^{2} + 1.5887T_{\exp} - 10.557 \qquad (2)$$

This correlation will be applied to previous experimental data points and documented in a future report.

Task 4 – Solvent Reclaiming

Subtask 4.1 – Sulfate Precipitation

Jason Davis

(Supported by this contract)

Introduction

This subtask will be used to define future work for the development of a MEA recovery technique designed to remove sulfate (SO_2) from a solution of MEA used for CO_2 capture. The goal of this work will be to develop an integrated CO_2 and SO_2 removal system that will be used in place of a separate flue-gas desulphurization (FGD) and CO_2 removal system. This should be a more cost-effective approach than the two separate units since the flue gas will only need to go through a single contactor to remove both species thereby reducing the capital and energy requirements necessary to run separate contactor systems.

In the proposed process, a slipstream of MEA rich in SO_2 will be diverted from the stripper outlet to a crystallization system where it will be mixed with solid $Ca(OH)_2$ to crystallize $CaSO_4$ from the solution. The MEA will then go through a solids removal step and a secondary crystallization to remove residual Ca^{++} ion from the solution. In the current work section, potassium sulfate crystallization is also characterized as a potential substitute for calcium sulfate.

Theory

Sulfate can be effectively removed from flue gas using an MEA stripper/absorber system like the one used to remove CO_2. The problem is that SO_2 binds more strongly with MEA and is not likely to be dissociated from the MEA in the stripper system under normal CO_2 removal conditions. As a result, SO_2 will build up in the MEA and decrease the effectiveness of CO_2 removal when enough is accumulated. The proposed process aims to address this problem.

An overview of the proposed crystallization system is shown below in Figure 16. The feed to this system will be a slipstream from the stripper outlet of the absorber/stripper system and will have to go through a secondary stripping step to further reduce the CO_2 loading of the solvent before reaching the first crystallization step.

The initial crystallization, as shown in CR-100 of Figure 16, involves the addition of solid calcium hydroxide to the incoming MEA in a CSTR crystallizer. The crystallization is defined by the following reaction.

$$(MEAH^{+})_2SO_4^{=} + Ca(OH)_{2(s)} \longrightarrow 2\ MEA(aq) + CaSO_{4(s)} + 2\ H_2O$$

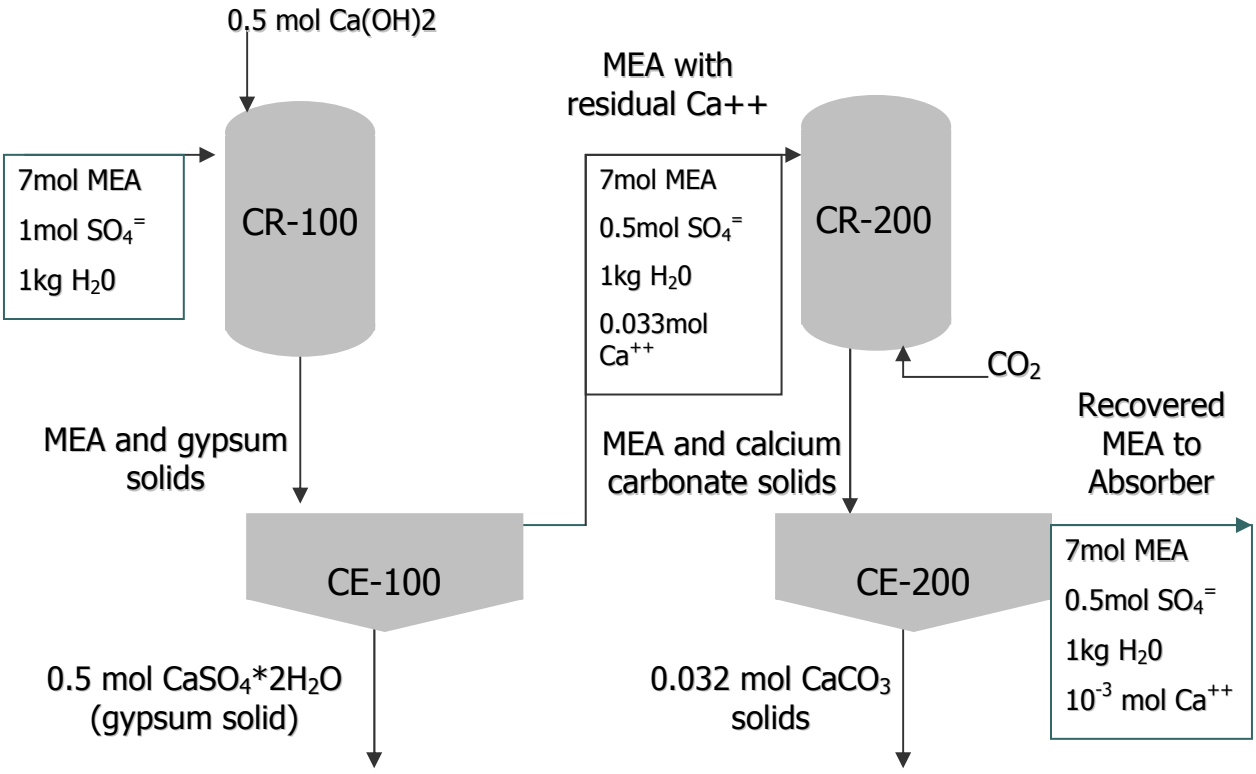

Figure 16: Process for the Removal of SO_2 from MEA by Crystallization.

The MEA and gypsum solids will then pass through a solids removal step, such as a centrifuge or cyclone, where the solids will be washed with water to remove as much MEA as possible and the solid waste will then be disposed. There will be residual Ca++ left in solution after the initial crystallization on the order of 0.033 mol/L based on the solubility of gypsum and calcium hydroxide in water (Linke, 1958). This residual calcium will need to be removed in order to prevent fouling in the absorber system. This will be achieved in the second crystallization step by bubbling CO_2 into the system to form $CaCO_3$ solids as governed by the following chemical reaction.

$$Ca^{++} + 2\,MEA + CO_2 + H_2O \longrightarrow CaCO_{3(s)} + 2\,MEAH^{+}$$

The MEA and calcium carbonate will have to be separated in a second solids removal system similar to the one used for gypsum crystallization, but on a much smaller scale, before the MEA can be returned to the absorber/stripper system. The amount of residual calcium should be much lower than the first crystallization as the solubility of calcium carbonate in pure water is 1.3×10^{-4} mol/L and 1.0×10^{-3} mol/L in a 0.9 mol K_2SO_4 solution (Linke, 1958).

Current Work

An initial set of laboratory runs from Richardson et.al. was meant to measure the effect of residence time on crystal size for the calcium sulfate crystallizer mentioned above. In the initial runs it was noticed that there was an inordinate amount of solids in the system at startup when it was expected that the calcium hydroxide would dissolve rather quickly but the gypsum crystallization would take time. A set of dissolution studies were then performed in a batch crystallizer by filtering the solids at the end of a 24 hour period washing with water and titrating with hydrochloric acid. It was shown by this method that only two-thirds of the calcium hydroxide dissolved over this time span.

Upon conclusion of the study by Richardson, experiments into the solubility of $Ca(OH)_2$ in 30wt% MEA solutions were performed using HCl and H_2SO_4 to maintain the pH at a desired level. 10g of calcium hydroxide were added to 100ml of MEA solution after the solution had been pH adjusted to the desired starting point. Figure 17 shows the dissolution curve for MEA using HCl as the titrant.

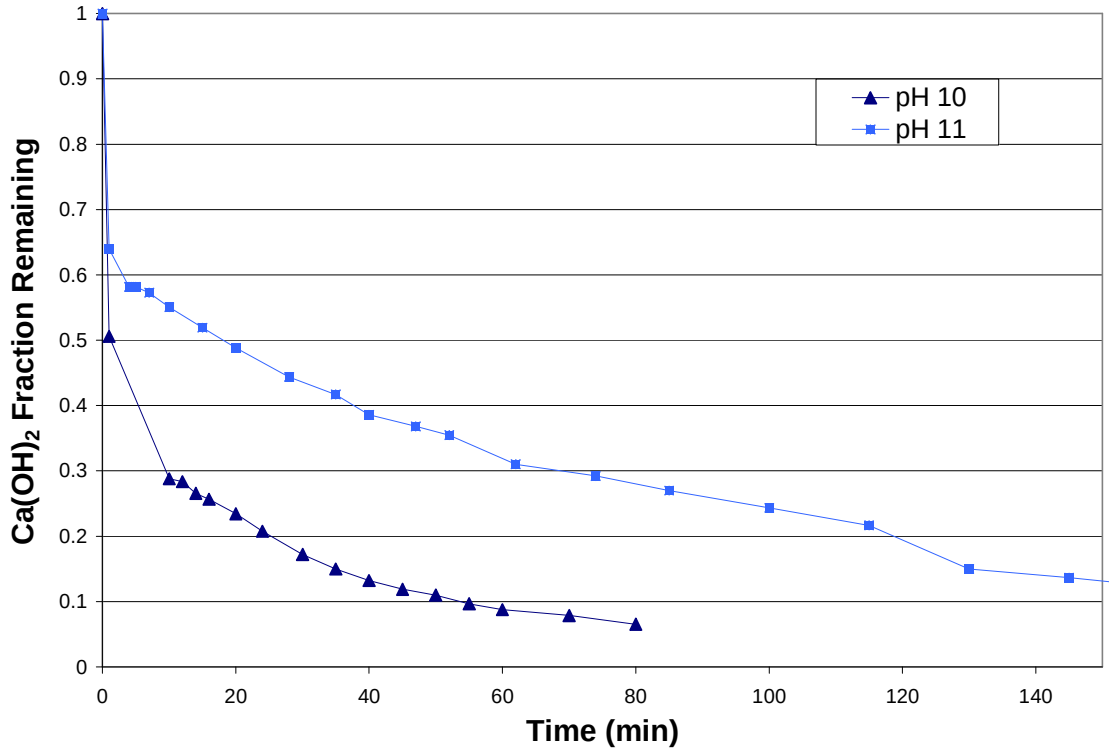

Figure 17: Dissolution of Calcium Hydroxide at Varying pH

As you can see from this graph, calcium hydroxide dissolution was more rapid at lower pH levels as expected. However, for each of the runs, calcium hydroxide fully dissolved in solution over a period of a few hours compared to the results of Richardson where only two thirds dissolved over the course of a day. When the experiment was repeated using sulfuric acid, the dissolution rate was so fast that it was not measurable by the given method. For the cases where

the pH was maintained at 10.0 and 11.0, the calcium hydroxide was fully dissolved in under 5 minutes.

Potassium sulfate crystallization is another potential system that is being analyzed for sulfate removal from MEA. In a study performed by Sachde and Sivaram, they tested the solubility of potassium sulfate in varying concentrations of MEA and MEA/Piperazine blends. It was found that K_2SO_4 solubility decreases with increasing amine concentration and has a slight temperature dependence showing increased solubility with increased temperature. They also performed tests on how loading affects solubility in the MEA/Piperazine blend and found that there was a drastic increase in solubility (~300% increase) in loaded versus unloaded solutions which may present an interesting phenomenon that may be used to our advantage in the sulfate removal process.

Future Work

The experiment by Richardson will be repeated to determine reproducibility and further experiments will be used to characterize the solids concentration of calcium hydroxide in the first crystallizer. Further studies on the affect of CO_2 loading on the solubility of potassium sulfate in pure MEA systems and MEA/Piperazine blends will also be performed.

Task 5 – Corrosion

Subtask 5.1 – Corrosion in base solution compared to MEA

By Amorvadee (Amy) Veawab

Associate Professor, University of Regina

Supported by subcontract

Research Objectives

The carbon dioxide (CO_2) absorption process using aqueous chemical solutions is subject to a number of operational difficulties, of which the most severe is corrosion of process equipment and solvent degradation. Corrosion problems have been receiving a great deal of attention because they have substantial impacts on the plant's economy, especially in terms of unplanned downtime, production losses, reduced equipment life, and extra-expenditure for restoring the corroded equipment and for treatment systems initiated to mitigate the corrosion. The corrosion problems also prevent the absorption process from achieving energy efficient operations.

The aqueous solution of blended potassium carbonate and piperazine has demonstrated to be a promising solvent for CO_2 capture from coal-fired power plant flue gas due to its capture performance and energy efficiency. It is our goal to further explore the promise of this solvent in an aspect of the potential operational problems. This project focuses on the investigation of corrosion of materials during CO_2 absorption and solvent regeneration in the presence and absence of solvent degradation products and chemical additives including oxidative inhibitors and corrosion inhibitors.

The research involves comprehensive literature review on the corrosion in CO_2 absorption process using potassium carbonate and piperazine, and experimental evaluations in the following sequences.

Task 1: Evaluation of corrosion in base solution (the blended potassium carbonate and piperazine) against the corrosion in an aqueous solution of monoethanolamine (MEA).

Task 2: Evaluation of corrosion in base solution containing degradation products.

Task 3: Evaluation of corrosion in base solution containing degradation products and oxidative inhibitors.

Task 4: Evaluation of inhibition performance of corrosion inhibitor in the presence of degradation products and oxidative inhibitors.

Justification for any deviations from original objectives

Based on our discussion with Dr. Rochelle, we would like to expand our project to cover the corrosion study in both K_2CO_3-piperazine and MEA-piperazine since MEA-piperazine is another promising piperazine-based solvent for the cost-effective CO_2 capture. The original tasks for K_2CO_3-MEA will be kept minimum, and the tasks with similar objectives will be carried out for MEA-piperazine system.

Progress made towards the objectives

Over the past three months, we have been conducting a series of short-term electrochemical corrosion experiments under various conditions to obtain corrosion rate of carbon steel and gain understanding of corrosion behavior in aqueous solutions of MEA and blended MEA-piperazine. Results and discussion are provided below.

Corrosion behavior of carbon steel in MEA and blended MEA-Piperazine

Carbon steel manifests active, passive and transpassive behavior depending upon the aggressiveness of electrolyte solution or the potential of net oxidation/ reduction reactions. As seen from Figure 18 and Figure 19, under the test conditions, carbon steel is clearly in active state where corrosion takes place at the corrosion potential (E_{corr}) and corrosion current density (i_{corr}). According to Pourbaix diagrams in Figure 20, Figure 21, Figure 22, Figure 23, Figure 24, and Figure 25, no passive film is developed to protect the metal surface. Fe^{2+} and $FeCO_3$ (aq) are stable in the aqueous solution as shown in below reactions.

$$Fe \rightarrow Fe^{2+} + 2e^- \quad (1)$$

$$Fe^{2+} + HCO_3^- \leftrightarrow FeCO_3 + H^+ \quad (2)$$

As the potential is increased beyond the primary passivation potential (E_{pp}), passive film passivates on the metal surface, and current density reduces substantially to passive current density (i_{pass}). As a result, corrosion can be reduced due to the formation of ferrous oxide (Fe_2O_3) as seen from the Pourbaix diagram and the reaction below.

$$2\,FeCO_3 + 4OH^- \rightarrow Fe_2O_3 + 2HCO_3^- + H_2O + 2\,e^- \quad (3)$$

The passive film then breaks down at transpassive potential (E_{trans}). All electrochemical kinetic parameters are listed in Table 10.

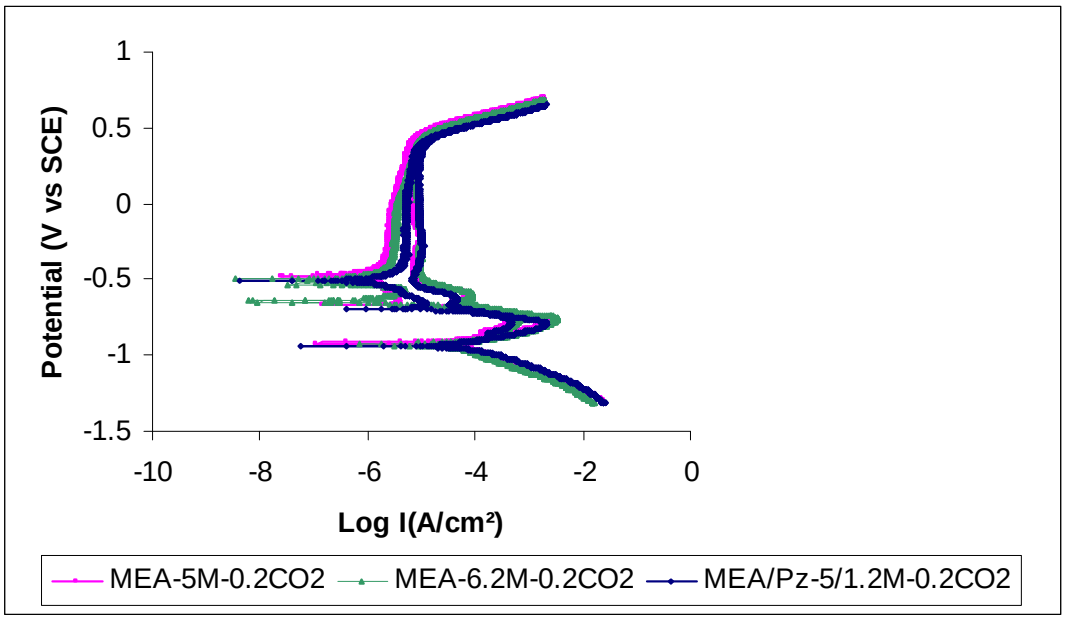

Figure 18: Cyclic polarization curves of MEA (5M and 6.2M) and blended MEA-piperazine (5M:1.2M) solutions containing 0.20 mol/mol CO_2 loading at 80°C.

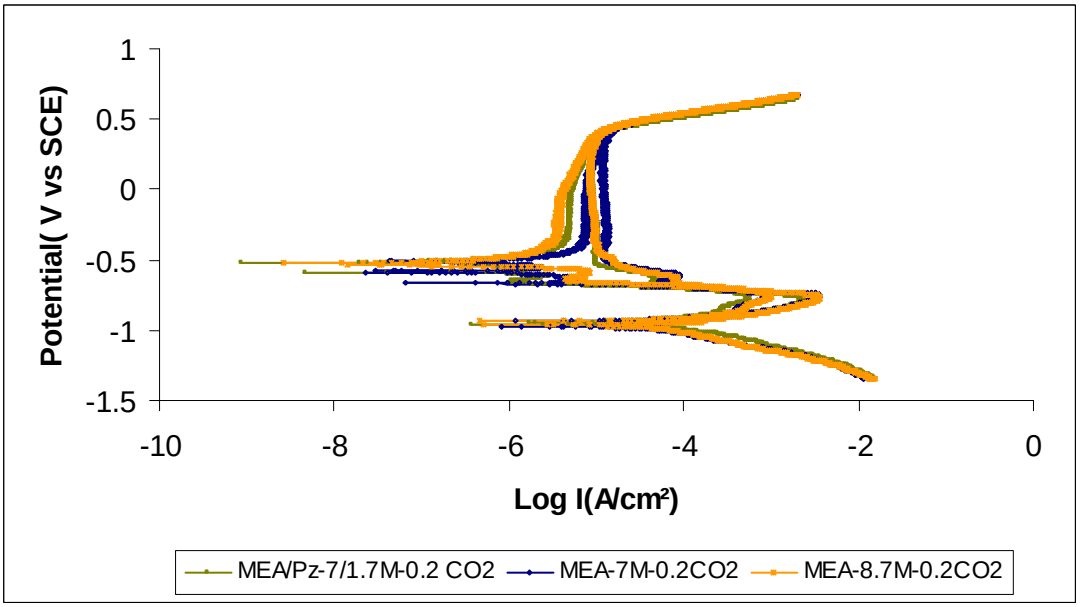

Figure 19: Cyclic polarization curves of MEA (7M and 8.7M) and blended MEA-piperazine (7M:1.7M) solutions containing 0.20 mol/mol CO_2 loading at 80°C.

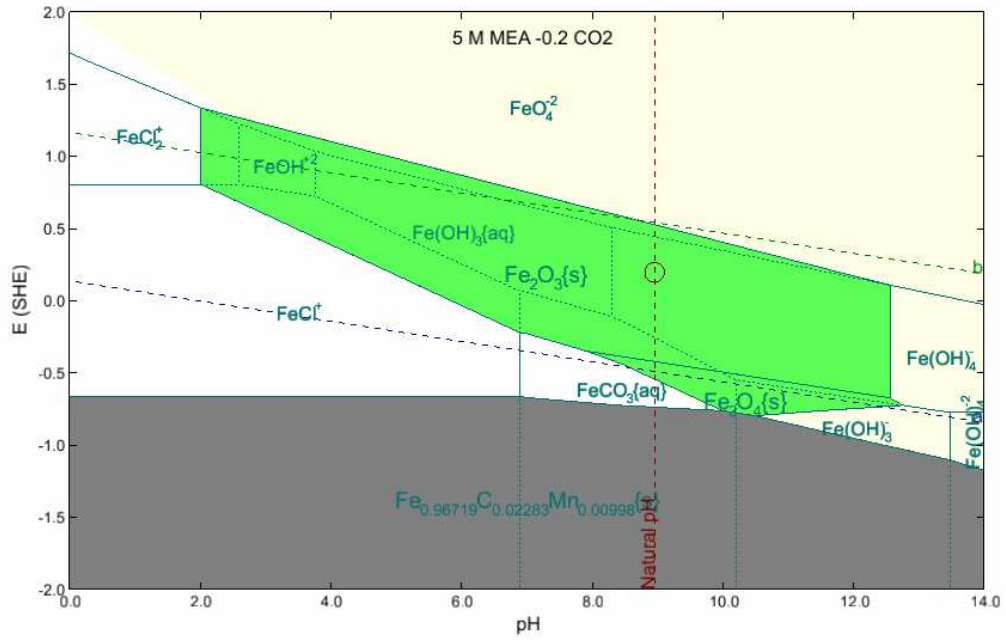

Figure 20: Pourbaix diagram of carbon steel in 5M MEA containing 0.20 mol/mol CO_2 loading at 80^{o}C.

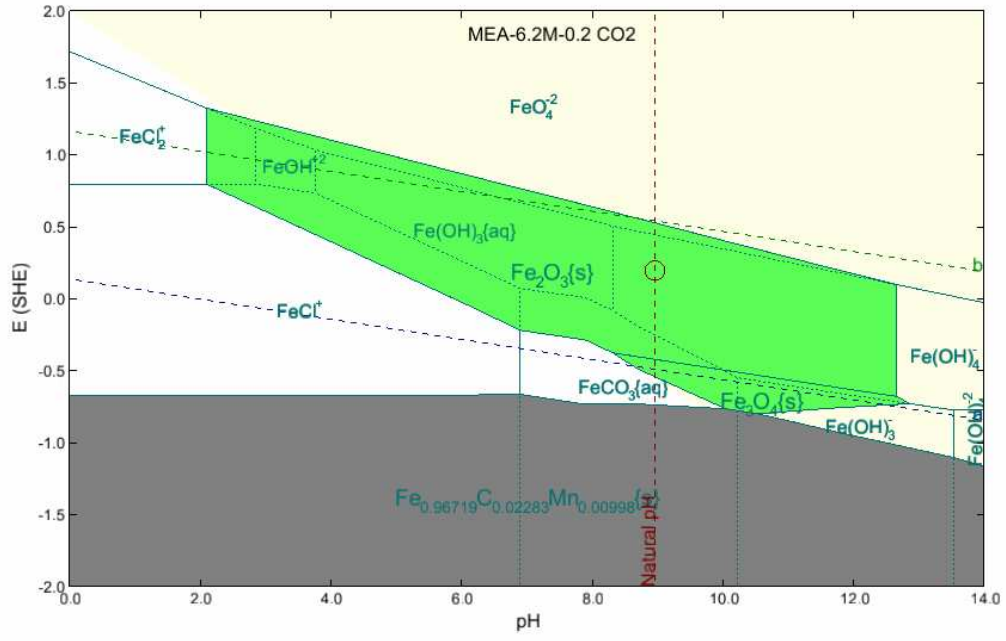

Figure 21: Pourbaix diagram carbon steel in 6.2M MEA containing 0.20 mol/mol CO_2 loading at 80^{o}C.

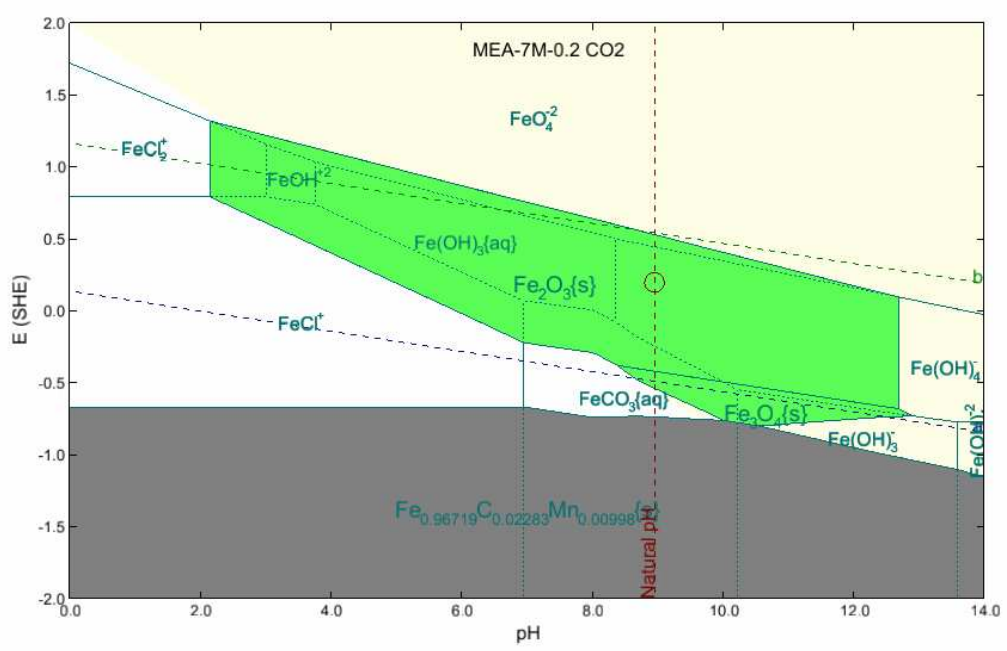

Figure 22: Pourbaix diagram of carbon steel in 7M MEA containing 0.20 mol/mol CO_2 loading at 80°C.

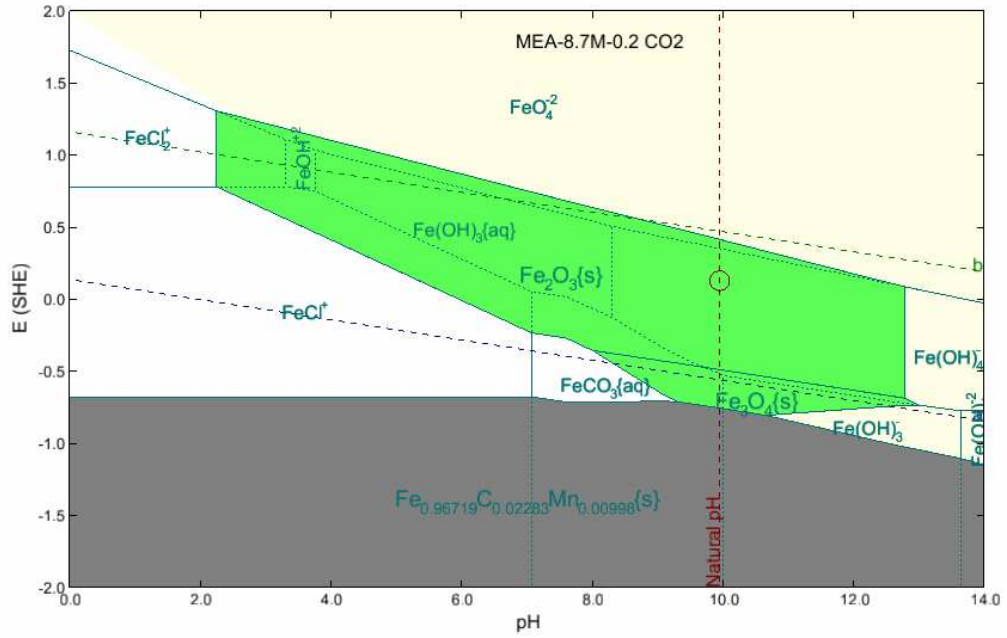

Figure 23: Pourbaix diagram of carbon steel in 8.7M MEA containing 0.20 mol/mol CO_2 loading at 80°C.

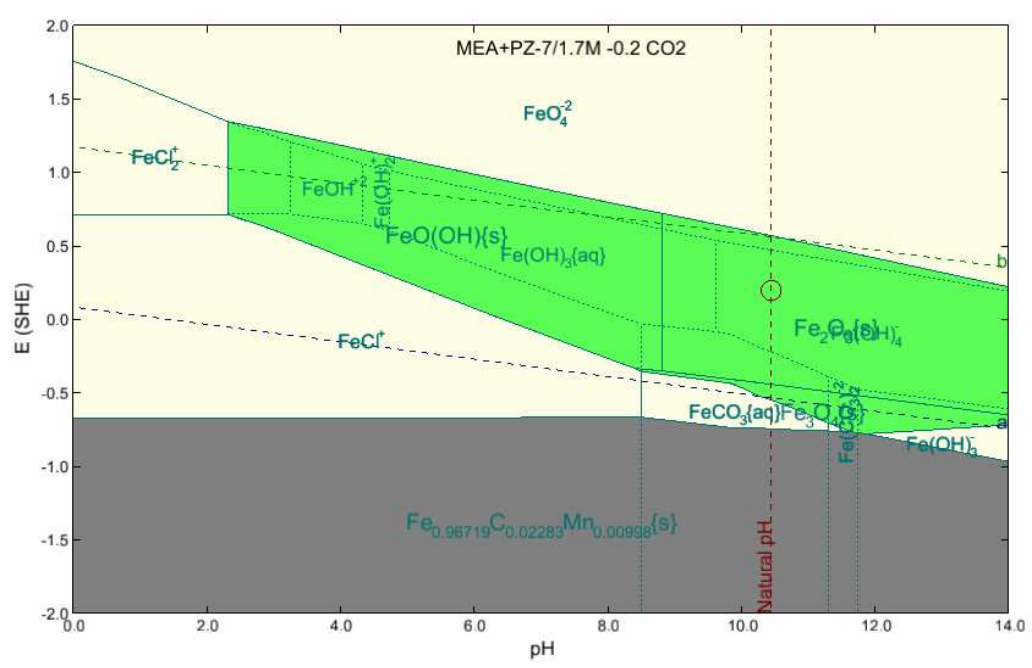

Figure 24: Pourbaix diagram carbon steel in 7M MEA-1.7M piperazine containing 0.20 mol/mol CO_2 loading at 80^{o}C.

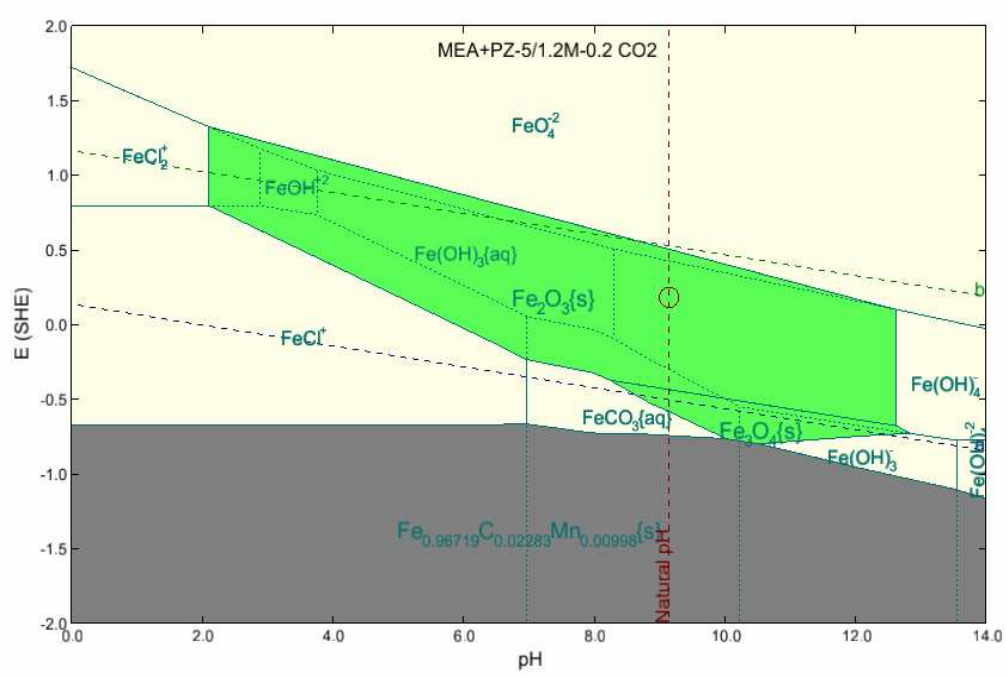

Figure 25: Pourbaix diagram of carbon steel in 5M MEA-1.2M piperazine containing 0.20 mol/mol CO_2 loading at 80^{o}C.

Table 10: Summary of electrochemical kinetic parameters

System	Ecorr	icorr	βa	βc	Epp	ic	ipass	Etrans	Ecp	Etrans-Ecp	Erp	Cor rate
	V	μA	mV/decade	mV/decade	V	A/cm²	A/cm²	V	V	V	V	(mpy)
MEA-5M-0.2CO2	-0.919	175.9	64.77	112.2	-0.753	-2.689	-5.129	0.434	-0.44	0.871	-0.477	16.2
MEA-6.2M-0.2CO2	-0.932	236.3	69.5	137.5	-0.743	-2.579	5.049	0.359	-0.41	0.764	-0.499	21.42
MEA-7M-0.2CO2	-0.975	236.3	95.76	124.7	-0.737	-2.539	-4.938	0.327	-0.44	0.764	-0.587	21.76
MEA-8.7M-0.2CO2	-0.963	286.4	83.45	146.9	-0.744	-2.549	-4.999	0.361	-0.39	0.749	-0.518	26.38
M+P-5/1.2M-0.2CO2	-0.94	240.7	79.94	108.3	-0.774	-2.869	-5.108	0.294	-0.46	0.749	-0.508	22.16
M+P-7/1.7M-0.2CO2	-0.959	382.3	90.97	138.2	-0.761	-2.749	-5.009	0.327	-0.42	0.748	-0.516	35.22
M+P-5/1.2M-satnCO2	-0.854	653.7	103.9	147.5	-0.618	-2.339	-4.619	0.44	-0.4	0.837	-0.416	60.2
M+P-7/1.7M-satnCO2	-0.834	1479	178.2	173.2	-0.593	-2.559	-4.929	0.519	-0.33	0.847	-0.416	136.2
M+P-7/1.7M-0.2CO2-10%O2*	-0.846	108	113.396	86.01	-0.64	-2.5	-4.417	0.494	-0.55	1.044	-0.262	16.4
M+P-7/1.7M-0.2CO2-10%O2	-0.87	106	91.522	127.228	-0.693	-2.618	-4.626	0.357	-0.53	0.882	-0.351	16.4

***** - 1000 rpm (rotation)

2. Effect of amine concentration on corrosion

Amine concentration has an apparent effect on corrosion. As seen from Figure 26, increasing amine concentration makes both MEA and MEA-piperazine systems more corrosive, and thus accelerates the corrosion rates of carbon steel. Such corrosiveness is caused by decreases in corrosion potential (E_{corr}),and changes in anodic (β_a) and cathodic (β_c) Tafel slopes, or changes in mechanism of iron dissolution and reduction of oxidizing agents. In passive region where the metal surface is passivated, increasing amine concentration does not affect the protection performance of the passive film. This is evidenced by insignificant changes in critical current density(i_c), primary passivation potential (E_{pp}) and passivation current density (i_p). However, the passive film can break down at a lower potential as the amine concentration increases.

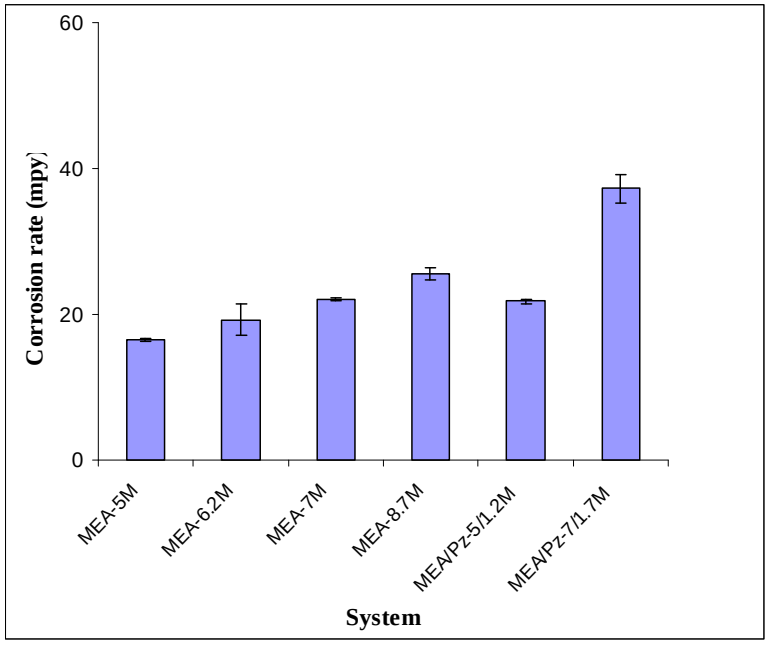

Figure 26: Comparison of corrosion rates of carbon steel in MEA and MEA-piperazine solutions containing 0.20 mol/mol CO_2 loading at 80^{o}C.

3. Effect of piperazine on corrosion

The blended MEA-piperazine solution is more corrosive than MEA solution. For instance in Figure 26, at 80^{o}C and 0.20 mol/mol CO_2 loading, corrosion rate of 6.2 M MEA is 19.23 mpy whereas that of 5 M MEA-1.2 M piperazine is 21.79 mpy. The effect of piperazine on corrosion is more pronounced when the total amine concentration is increased to 8.7 M. This can be explained by changes in anodic and cathodic Tafel slopes or changes in mechanism of iron dissolution and reduction of oxidizing agents. The transpassive potential (E_{trans}) value also decreases from 0.361 to 0.294 V in the presence of piperazine, which could mean that the protective film formed in the presence of piperazine is not as stable as that of MEA.

4. Effect of CO_2 loading on corrosion

Blended MEA-piperazine solutions containing 0.20 mol/mol CO_2 loading and CO_2 saturation were used for examining the effect of CO_2 loading on corrosion. The results in Figure 27, Figure 28, and Figure 29 show that CO_2 loading has a significant effect on corrosion rate of carbon steel. Higher CO_2 loading causes the solution to be more corrosive. For instance, in 5M MEA-1.2M piperazine at 80^{o}C, the corrosion rate of carbon steel increases from 22 to 60 mpy when the CO_2 loading is increased from 0.20 mol/mol to saturation. Such CO_2 loading effect is found to be more pronounced at a higher amine concentration, e.g. in 7M MEA-1.7M piperazine, the corrosion rate increases from 36 to 136 mpy. The increasing corrosion rate is due to the increases in anodic and cathodic Tafel slopes or changes in mechanism of iron dissolution and reduction of oxidizing agents. It should be noted that the active species participating in corrosion process are similar to the system containing 0.20 mol/mol CO_2 loading. As illustrated in Figure 30 and Figure 31, $FeCO_3$ is stable in the active state, while Fe_2O_3 is a passive film in the passive state.

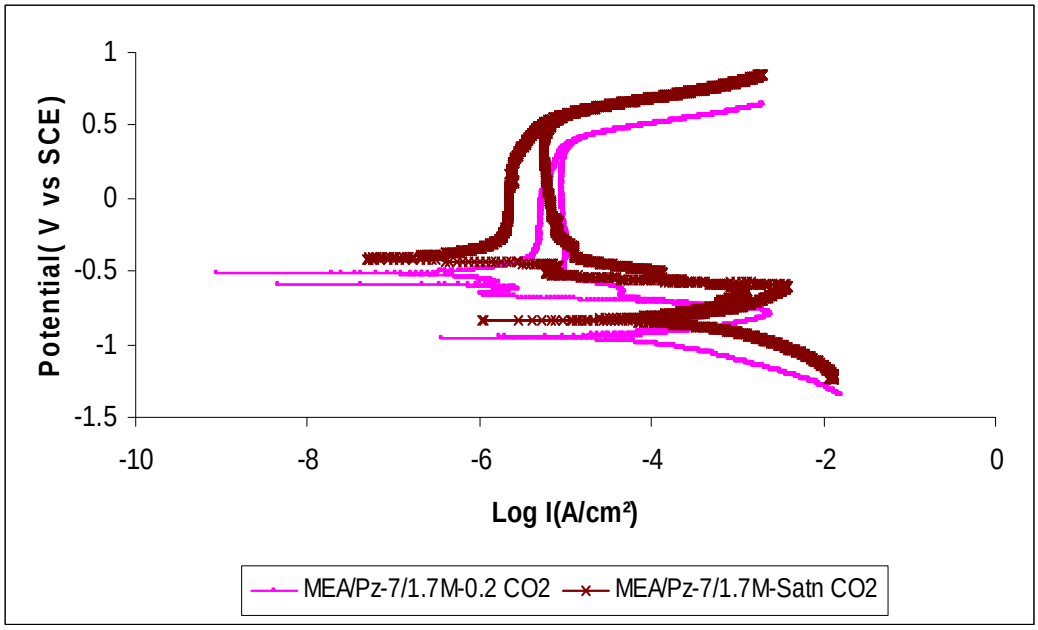

Figure 27: Cyclic polarization curves of carbon steel in 7 M MEA+1.7M piperazine solution containing 0.2 mol/mol CO_2 loading and Saturation CO2 loading.

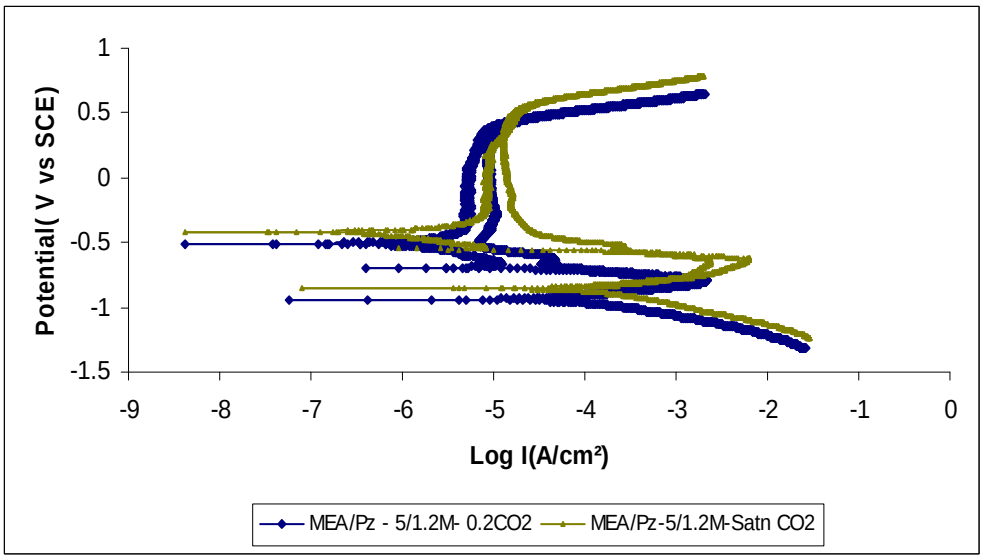

Figure 28: Cyclic polarization curves of carbon steel in 5M MEA-1.2M piperazine solution containing 0.20 mol/mol CO_2 loading and saturation CO2 loading.

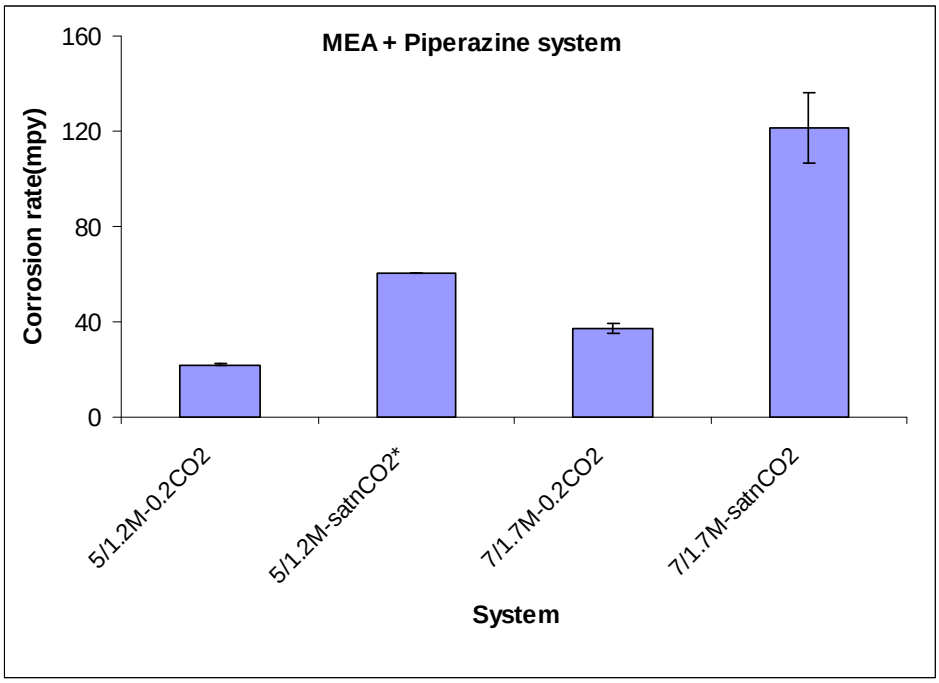

* pitting tendency

Figure 29: Comparison of Corrosion rates of carbon steel in blended MEA-piperazine solution containing different CO_2 loadings.

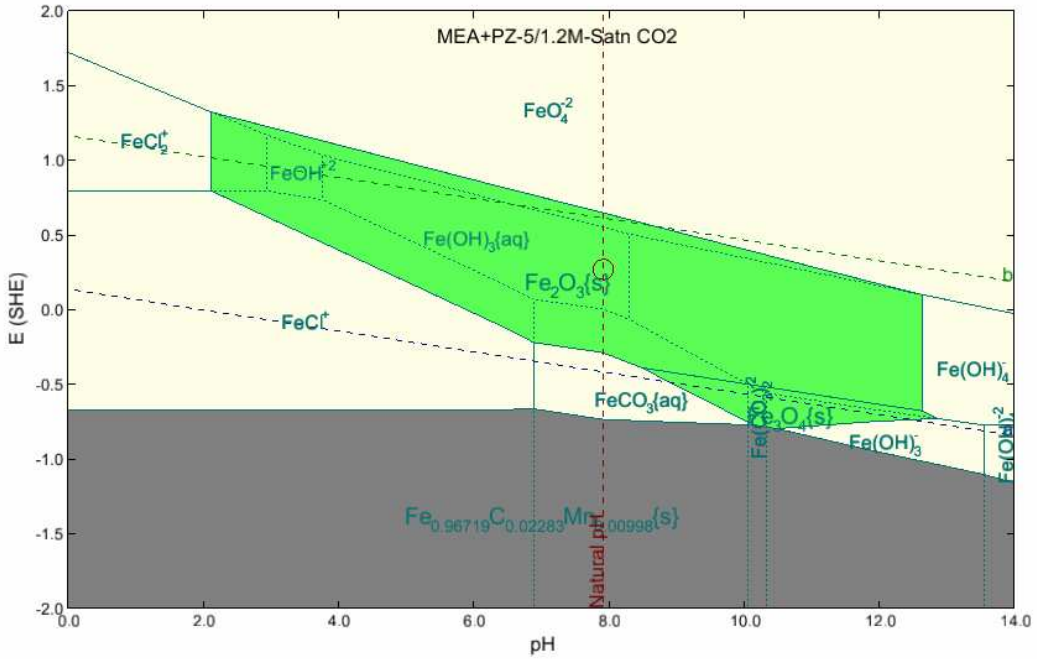

Figure 30: Pourbaix diagram of carbon steel in 5M MEA-1.2 M piperazine solution containing CO_2 saturation.

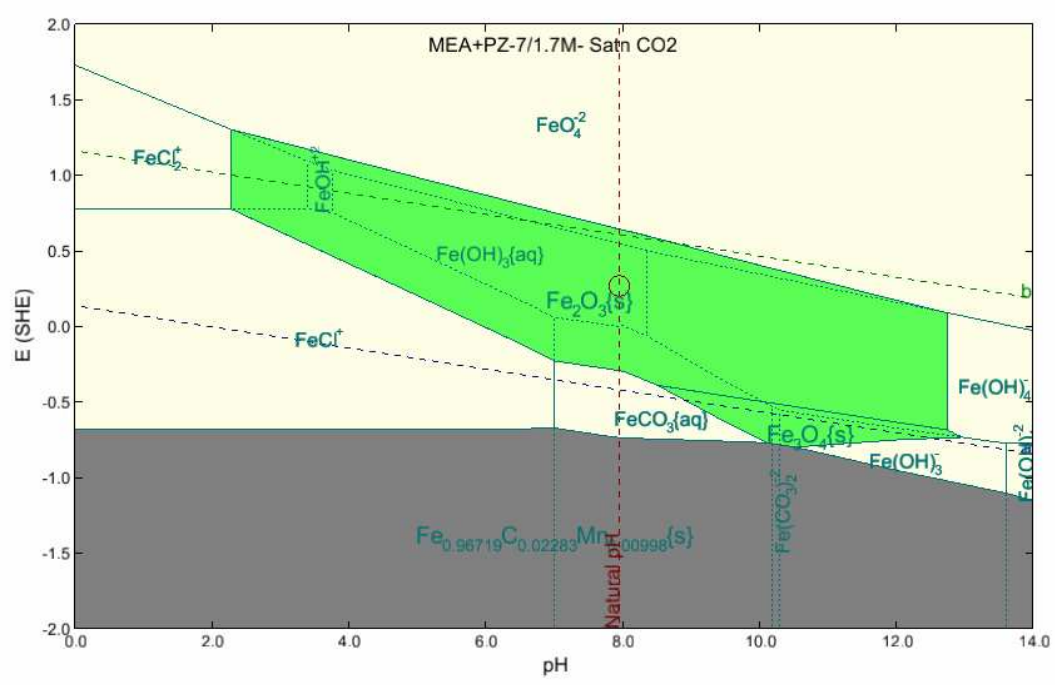

Figure 31: Pourbaix diagram of carbon steel in 7M MEA-1.7 M piperazine solution containing CO_2 saturation.

5. Effect of solution velocity on corrosion

The corrosion experiments were carried out in a micro-cell with a rotating speed of 1,000 rpm to determine the effect of solution velocity. The aqueous solutions of 7M MEA-1.7M piperazine containing 0.20 mol/mol CO_2 loading under 10% oxygen in gas were used. The results in Figure 32 and Figure 33 show that the solution velocity has negligible effect on corrosion rate. This means that there is no mass-transfer limitation of the active species involved in corrosion process. The anodic and cathodic Tafel slopes slightly change.

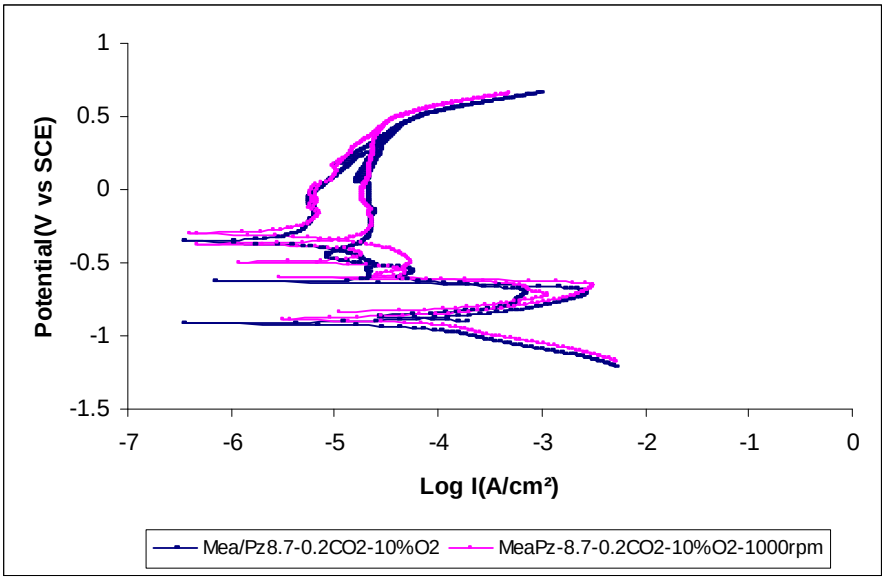

Figure 32: Cyclic polarization curves of carbon steel in 7M MEA-1.7 M piperazine containing 0.20 CO_2 under 10% O_2.

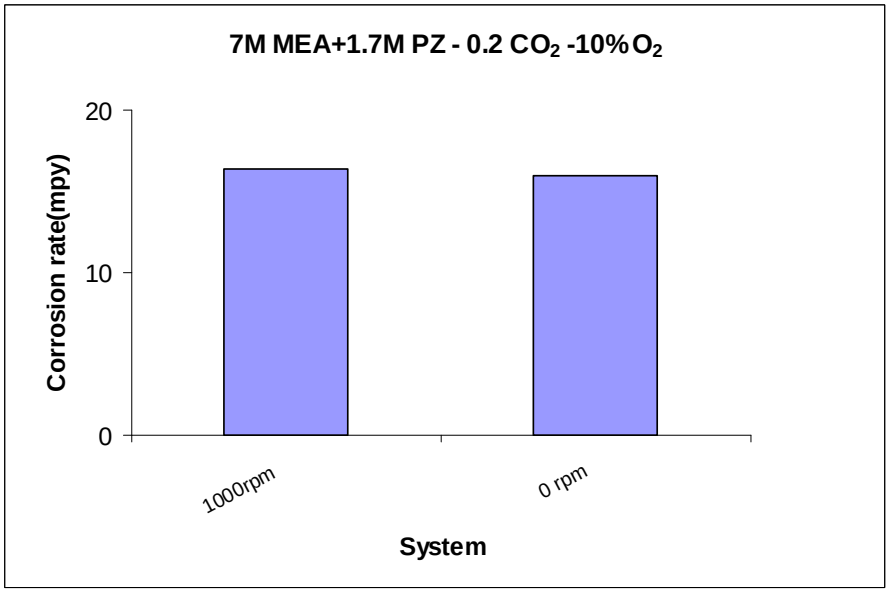

Figure 33: Comparison of corrosion rates of carbon steel in 7M MEA-1.7 M piperazine solution containing 0.20 CO_2 loading under 10 % O_2 in gas.

References

Blezard, Michael; Jones, Glyn R. Nitrosamine inhibition. United States Patent Application No. 5,223,644. 1993.

Calle, Emilio; Casado, Julio; Cinos, Jose L.; Garcia Mateos, Francisco J.; Tostado, Manuel. Formation of nitrosamines in alkaline conditions: a kinetic study of the nitrosation of linear and cyclic secondary amines by nitroalkanes. Journal of the Chemical Society, Perkin II, 1559-1564, 1992.

Challis, B.C.; Challis, J.A. *N*-nitrosamines and *N*-nitrosoimines, p. 1151-1223, The chemistry of amino, nitroso and nitro compounds and their derivatives, Supplement F, Part 2, edited by S. Patai, John Wiley and Sons, New York, 1982.

Challis, B.C.; Kyrtopoulos, S.A. The Chemistry of Nitroso-compounds. Part 11. Nitrosation of amines by the two-phase interaction of amine in solution with gaseous oxides of nitrogen. J. Chem. Soc., Perkin I, 1979.

Chen, C. C.; Evans, L. B., A local composition model for the excess Gibbs energy of aqueous electrolyte systems. AIChE Journal 1986, 32, (3), 444-54.

Cullinane, J. T. Thermodynamics and Kinetics of aqueous piperazine with potassium carbonate for carbon dioxide absorption. Ph.D Dissertation, University of Texas-Austin, Austin, 2005.

Dawson, Brian A.; Lawrence, Robert C. Analysis of piperazine drug formations for *N*-nitrosamines. Journal – Association of Official Analytical Chemists, 70(5), p. 840-841, 1987.

Dionex IonPac CS17 Analytical Column Product Manual. Revision 03. May 2003. http://www1.dionex.com/en-us/webdocs/manuals/ic/31747-03_CS16_V19.pdf (Accessed January 2005)

Elespuru, R.K.; Lijinsky, W. Mutagenicity of cyclic nitrosamines in *Escherichia coli* following activation with rat liver microsomes. Cancer Research, p. 4099-4101, 1976.

Freguia, S.; Rochelle, G. T., Modeling of CO2 Capture by Aqueous Monoethanolamine. AIChE Journal 2003, 49, (7), 1676-1686.

Goff, G. S.; Rochelle, G. T. Monoethanolamine Degradation: O2 Mass Transfer Effects under CO2 Capture Conditions. Industrial & Engineering Chemistry Research 2004, 43(20), 6400-6408.

Hilliard, M.D. "Thermodynamics of aqueous piperazine/potassium carbonate/carbon dioxide characterized by the electrolyte NRTL model with Aspen Plus." Master's Thesis, Department of Chemical Engineering, The University of Texas at Austin, Austin, TX, 2005.

Keefer, L.K.; Roller, P.P. *N*-Nitrosation by Nitrite Ion in Neutral and Basic Medium, Science 181, 1245-47, 1973.

Kirsch, Michael; Korth, Hans-Gert; Sustmann, Reiner; De Groot, Herbert. Carbon Dioxide but Not Bicarbonate Inhibits *N*-Nitrosation of Secondary Amines. Evidence for Amine Carbamates as Protecting Entities. Chemical Research in Toxicology, 13(6), p. 451-461, 2000.

Klein, R.G. Calculations and measurements on the volatility of *N*-nitrosamines and their aqueous solutions. Toxicology, 23(2-3), 135-147, 1982.

Linke, W.F., Seidell, A., Solubilities, Inorganic and Metal-Organic Comounds, D. Van Nostrad Company Inc., Princeton, NJ, 1958.

Love, L.A.; Lijinsky, W.; Keefer, L.; Garcia, H. Chronic oral administration of 1-nitrosopiperazine in high doses to MRC rats. *Z. Krebsforsch*., p. 69-73, 1977.
Lovejoy, D.J.; Vosper, A.J. Part VI. The Reaction of Dinitrogen Trioxide with Primary and Secondary Amines, J. Chem. Soc. (A), 2325-2328, 1968.
Mock, B.; Evans, L. B.; Chen, C. C., Thermodynamic representation of phase equilibria of mixed-solvent electrolyte systems. AIChE Journal 1986, 32, (10), 1655-64.
Onda, K.; Takeuchi, H.; Okumoto, Y., Mass transfer coefficients between gas and liquid phases in packed columns. Journal of Chemical Engineering of Japan 1968, 1, (1), 56-62.
Oyenekan, B. A.; Rochelle, G. T., Energy Performance of Stripper Configurations for CO2 Capture by Aqueous Amines. Ind Eng Chem Res 2006, 45, (8), 2457-64.
Oyenekan, B. A.; Rochelle, G. T., Alternative Stripper Configurations to Minimize Energy for CO2 Capture. In 8th International Conference on Greenhouse Gas Control Technologies, Trondheim,Norway, 2006.
Richardson, B., Schussler, E., and Silver, M., "Regeneration of Monoethanolamine by Gypsum Crystallization for Carbon Capture Systems", University of Texas - CHE 264 Undergraduate Special Project, Spring 2006.
Rochelle, G. T. Personal Communication to Andrew Sexton. Austin, TX, 2005.
Sachde, D., and Sivaram, S., "CO_2 Capture: Solubility of Potassium Sulfate in Amine Solutions", University of Texas - CHE 264 Undergraduate Special Project, Summer 2006
Shoulders, B. Personal Communication to Andrew Sexton. Austin, TX, 2005.
Smith, P.A.S.; Loeppky, R.N. Nitrosative Cleavage of Tertiary Amines, J, ACS, 89, 1147-1157, 1967.
Talzi, V.P., "NMR Determination of the Total Composition of Commercial Absorbents Based on Monoethanolamine", *Russian Journal of Applied Chemistry*, 2004, 77(3), 437-441.
Tobiesen, F. A.; Svendsen, H. F.; Hoff, K. A., Desorber energy consumption in amine based absorption plants. Int. J of Green Energy 2005, 2, 1-15.
Tricker, A.R.; Kumar, R.; Siddiqi, M.; Khuroo, M.S.; Preusmann, R. Endogenous formation of *N*-nitrosamines from piperazine and their urinary excretion following antihelmintic treatment with piperazine citrate. Carcinogenesis, 12(9), p. 1595-1599, 1991.
Wang, J. Personal Communication to Andrew Sexton. Austin, TX, 2005.
Weiland, R. H.; Rawal, M.; Rice, R. G., Stripping of carbon dioxide from monoethanolamine solutions in a packed column. AIChE Journal 1982, 28, (6), 963-73.